TECH. MEMO
AERO 2137

UNLIMITED

TECH. MEMO
AERO 2137

ROYAL AEROSPACE ESTABLISHMENT

NUMERICAL EVALUATION OF A SOLUTION REPRESENTING A JET IN CROSS-FLOW

by

C. C. Lytton
J. H. B. Smith

August 1988

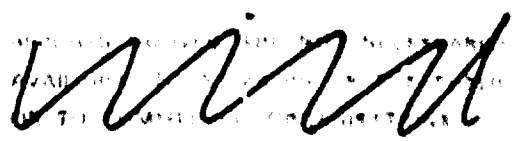

Procurement Executive, Ministry of Defence
Farnborough, Hants

UNLIMITED

ROYAL AEROSPACE ESTABLISHMENT

Technical Memorandum Aero 2137

Received for printing 4 August 1988

NUMERICAL EVALUATION OF A SOLUTION REPRESENTING A JET IN CROSS-FLOW

by

C. C. Lytton

J. H. B. Smith

SUMMARY

A recent study by Needham, Riley and Smith of a jet emerging from a circular pipe into a weak cross-flow under the assumptions of an inviscid and incompressible fluid led to expressions for the velocity potential in different regions near the orifice as definite integrals and infinite sums. In the present paper the expressions relating to flow inside the pipe and jet are evaluated with great care. It is confirmed that the solutions in the pipe and jet are continuous across the orifice plane. The behaviour of the solution near the orifice is displayed in graphical form, with emphasis on the consequences of the failure to satisfy a Kutta condition of smooth outflow at the lip.

LIST OF CONTENTS

1 INTRODUCTION

Needham, Riley and Smith[1] present an analysis of an idealized form of the jet-in-crossflow problem. The flow is assumed to be inviscid and incompressible. A jet emerges from a semi-infinite pipe in the shape of a circular cylinder into an ambient flow whose component normal to the pipe axis is small compared with the jet speed. The configuration is illustrated in Fig 1. The flow is irrotational both inside and outside the jet boundary, which forms a vortex sheet. This sheet is assumed to lie close to the circular cylinder defined by extending the pipe, so that the conditions of tangential flow and continuity of pressure which are satisfied on the jet boundary can be transferred to the cylinder.

The solution obtained is in two parts, corresponding to different length scales. If the ratio of the cross-flow velocity component to the jet speed is $\varepsilon \ll 1$, and the pipe radius is a, the first part of the solution, corresponding to a length scale of a/ε, is obtained as the first few terms of a power series in εx, where $x = \bar{x}/a$ and $\bar{x}$ is the distance from the exit plane. The second part, on a length scale of a, matches the first part to conditions at the pipe exit. This is obtained by the Wiener-Hopf technique, which leads to involved expressions for the velocity potential in distinct regions, *viz* inside the pipe, inside the jet, outside the jet and outside the pipe.

These expressions are so elaborate that there is no obvious way to confirm analytically that they satisfy the required conditions of continuity across the boundaries of the regions. Nor is it possible to deduce any quantitative information about the solution by inspection. Since there is at present very little known, in a mathematical sense, about the behaviour of jets in cross-flow, it seems worth investigating the behaviour of this model, physically unrealistic though it be. Accordingly, an attempt has been made to evaluate numerically the expressions obtained, first to confirm that the appropriate quantities are indeed continuous, and then to display the quantitative nature of the solution near to the pipe orifice.

It emerges that the numerical evaluation is far from straightforward; the typical task is to evaluate an integral, over an infinite range, of products of quasi-periodic functions (changing sign infinitely often) and a function which is itself defined by a further integration. For the particular case in which the coflowing component of the ambient stream is equal to the jet velocity, *ie* $\lambda = 1$ in Fig 1, one of the quasi-periodic functions reduces to a form which is more

amenable to numerical integration, and so the present exercise has been confined to this case. The restriction to $\lambda = 1$ does remove some of the physical content of the problem, in particular implying that the inclination of the jet to the ambient stream, $\tan^{-1}(\epsilon/\lambda)$, is small. Nonetheless, the particular case is believed to provide an adequate test of the analysis and a useful indication of the behaviour of the solution. Even for this case, considerable care and appreciable computing time are required, so it is thought worthwhile to place the methods and the results on record.

2 SUMMARY OF THE ANALYTIC SOLUTION NEAR THE ORIFICE

In Ref 1 is discussed the situation of an incompressible, inviscid fluid emerging with unit average speed from a long straight pipe of circular cross-section with unit radius. (So velocities and distances are scaled on pipe flow speed and pipe radius.) The jet emerges into a stream of similar fluid which has undisturbed velocity components λ parallel to the pipe and ϵ perpendicular to it, as indicated in Fig 1. Cylindrical polar coordinates (r,θ,x) are taken aligned with the pipe, with the origin at the centre of the pipe orifice, x directed out of the pipe and θ measured from the pipe leeward generator. Thus the pipe surface is given by $r = 1$, $x \leqslant 0$.

Since the cross-flow parameter ϵ is small, it is assumed that near the orifice the extension of the pipe ($r = 1$, $x \geqslant 0$) can be used to separate the representations of the flow. In equation (3-23) of Ref 1 the velocity potential ϕ in $r \geqslant 1$ is expanded formally in powers of ϵ. This expansion may be written as

$$\phi = \lambda x + \epsilon\left(r + \frac{1}{r}\right)\cos\theta + \epsilon^2\left[\psi_0(r,x) + \psi_2(r,x)\cos 2\theta\right] + O\left(\epsilon^3\right) , \quad (1)$$

and the potential $\tilde{\phi}$ in $r \leqslant 1$ is similarly expanded as:

$$\tilde{\phi} = x + \epsilon^2\left[\tilde{\psi}_0(r,x) + \tilde{\psi}_2(r,x)\cos 2\theta\right] + O\left(\epsilon^3\right) . \quad (2)$$

Here ψ_0, $\tilde{\psi}_0$ are functions giving the axially symmetric part of the solution, which will not concern us further, and ψ_2, $\tilde{\psi}_2$ give the part of the solution depending on θ, to this second order. In a small change of notation from Ref 1, a factor $\cos 2\theta$ has been taken out.

For the region inside the pipe, $x \leqslant 0$ and $r \leqslant 1$, the solution for $\tilde{\psi}_2$ is obtained from equation (3-36) of Ref 1 as:

$$\tilde{\psi}_2(r,x) = \left(\frac{2}{1+\lambda^2}\right)^{\frac{1}{2}} \sum_{n=1}^{\infty} \frac{J_2\left(\Omega_n r\right)\exp\left(-\Omega_n|x|\right)}{\Omega_n^3\,\bar{K}_+\left(i\Omega_n\right)J_2''\left(\Omega_n\right)}\left(1 + A\Omega_n\right) , \qquad (3)$$

where the summation is over the positive zeros Ω_n of $dJ_2(p)/dp \equiv J_2'(p) = 0$, where J_2 is the Bessel function of the first kind and second order. To define $\bar{K}_+$, we first introduce a function $\gamma(s)$ of the complex variable s:

$$\gamma = \gamma(s) = \lim_{\delta \to 0+} (s + i\delta)^{\frac{1}{2}}(s - i\delta)^{\frac{1}{2}}$$

where branch cuts are taken from $\pm i\delta$ to $\pm i\infty$, and the square-root branches are chosen to have positive real parts for s real. Hence, when $s = \omega$ is real, $\gamma = |\omega|$. Then, from the equations (B-13), (B-16) and (B-15) of Ref 1:

$$\bar{K}(s) = \frac{1}{\gamma}\left[\frac{I_2(\gamma)}{I_2'(\gamma)} - \lambda^2\,\frac{K_2(\gamma)}{K_2'(\gamma)}\right] \qquad (4)$$

$$F_{\pm}(s) = \pm\frac{1}{2\pi i}\int_{C_{\pm}} \frac{d\omega}{\omega - s}\,\lim\left[\frac{\gamma(\omega)\bar{K}(\omega)}{1+\lambda^2}\right] \qquad (5)$$

$$\bar{K}_{\pm}(s) = \left(1+\lambda^2\right)^{\frac{1}{2}} \lim_{\delta \to 0+} \frac{\exp\left[F_{\pm}(s) \pm \frac{i\pi}{4}\right]}{\left(s \pm i\delta\right)^{\frac{1}{2}}} \qquad (6)$$

where the upper or lower signs are to be taken throughout. $\bar{K}_-$ is needed later. Here I_2 and K_2 are modified Bessel functions of the first and second kinds respectively, and C_+, C_- are contours of integration lying respectively below and above all singularities in the complex ω-plane. In the following section it emerges that the contours can be taken to lie along the real axis. Finally, A is given as the quotient of two integrals:

$$A = \frac{\bar{C}_1}{\bar{C}_2} , \qquad (7)$$

where $$\bar{C}_1 = \int_0^\infty \frac{dp}{p} . i\hat{K}(p) . J_2'(p) . \bar{K}_+(ip) \ , \qquad (8)$$

$$\bar{C}_2 = \int_0^\infty dp \left[i\hat{K}(p) . J_2'(p) . \bar{K}_+(ip) + \frac{2}{\left(1 + \lambda^2\right)^{\frac{1}{2}}} p^{-\frac{1}{2}} \right] \qquad (9)$$

in which, since p is real and positive, we have from (B-19) of Ref 1:

$$i\hat{K}(p) = 2.\mathrm{Re}\left\{ \frac{iK_2'(-ip)}{D(-ip)} \right\} \qquad (10)$$

where Re denotes the real part of a complex function, and for convenience, we have introduced:

$$D(-ip) = I_2(-ip)K_2'(-ip) - \lambda^2 K_2(-ip)I_2'(-ip) \ . \qquad (11)$$

We have used $I_2(ip) = I_2(-ip)$ and $I_2'(ip) = -I_2'(-ip)$, see Ref 2.

For the region inside the jet, $x \geqslant 0$ and $r \leqslant 1$, the solution for $\tilde{\psi}_2$ is obtained from equation (3-38) of Ref 1, after correcting a misprint in the sign of Ap, as:

$$\tilde{\psi}_2(r,x) = -\frac{xr^2}{1 + \lambda^2} - \frac{1}{\pi\sqrt{2}\left(1 + \lambda^2\right)^{\frac{1}{2}}} \int_0^\infty \frac{dp}{p^2} . i\hat{K}(p) . J_2(pr) . \bar{K}_-(-ip) . e^{-px} . (1 - Ap)$$

..... (12)

For the region outside the jet, $x \geqslant 0$ and $r \geqslant 1$, the solution for ψ_2 is obtained from equation (3-42) of Ref 1 as:

$$\psi_2(r,x) = \frac{\lambda x}{\left(1 + \lambda^2\right)r^2} - \frac{\lambda}{\pi\sqrt{2}\left(1 + \lambda^2\right)^{\frac{1}{2}}}$$

$$\int_0^\infty \frac{dp}{p^2} . 2\ \mathrm{Re}\left\{ \frac{K_2(-ipr)}{D(-ip)} \right\} . \bar{K}_-(-ip) . iI_2'(ip) . e^{-px} . (1 - Ap) \qquad (13)$$

For the region outside the pipe, $x \leqslant 0$ and $r \geqslant 1$, the solution for ψ_2 is obtained from equation (3-40) of Ref 1 as:

$$\psi_2(r,x) = -\frac{\lambda}{\pi\sqrt{2}\left(1+\lambda^2\right)^{\frac{1}{2}}} \int_0^\infty \frac{dp}{p^3} .2\ \mathrm{Re}\left\{\frac{K_2(-ipr)}{K_2'(-ip)}\right\} \left\{\frac{e^{-p|x|}}{\bar{K}_+(ip)} .(1+Ap)\right. \qquad (14)$$

3 PRELIMINARY MANIPULATIONS

The Bessel functions, and modified Bessel functions, of orders 0 and 1 with real and positive arguments, are available as subroutines in the NAG Fortran Library. To obtain the functions of order two, and their derivatives, we can use the following properties given in Ref 2, which hold for integers $\nu \geqslant 1$:

$$J_{\nu+1}(z) = \frac{\overline{2\nu}}{z} J_\nu(z) - J_{\nu-1}(z) \qquad (15)$$

$$Y_{\nu+1}(z) = \frac{\overline{2\nu}}{z} Y_\nu(z) - Y_{\nu-1}(z) \qquad (16)$$

$$I_{\nu+1}(z) = I_{\nu-1}(z) - \frac{\overline{2\nu}}{z} I_\nu(z) \qquad (17)$$

$$K_{\nu+1}(z) = K_{\nu-1}(z) + \frac{\overline{2\nu}}{z} K_\nu(z) \qquad (18)$$

$$J_\nu'(z) = \tfrac{1}{2}\left[J_{\nu-1}(z) - J_{\nu+1}(z)\right] \qquad (19)$$

$$Y_\nu'(z) = \tfrac{1}{2}\left[Y_{\nu-1}(z) - Y_{\nu+1}(z)\right] \qquad (20)$$

Also the Bessel functions are related to the modified Bessel functions by way of:

$$I_\nu(-iz) = (-i)^\nu J_\nu(z) \qquad (21)$$

$$K_\nu(-iz) = \frac{\pi}{2} i^{\nu+1}\left[J_\nu(z) + i\, Y_\nu(z)\right] . \qquad (22)$$

Equations (3), (8), (9), (12), (13) and (14) show that we require $\bar{K}_{\pm}(\pm ip)$ and therefore $F_{\pm}(\pm ip)$, with p real and positive. In equation (5), taking the plus sign and putting $s = ip$, gives the singularity at $\omega = s$ in the upper half ω-plane so that C_+ (which must lie below it) can be taken to be the real axis; taking the minus sign and putting $s = -ip$, gives the singularity in the lower half-plane, so that C_- (which must lie above it) can again be taken to be the real axis. If $p = 0$, the contour must be indented at the origin.

From equation (4), $\bar{K}(s)$ is a real and even function of real s, so taking $C_{\pm}$ to be the real axis in equation (5) and taking upper or lower signs throughout, we have: ddd

$$F_{\pm}(\pm ip) = \pm \frac{1}{2\pi i} \int_{-\infty}^{\infty} \frac{d\omega}{\omega \mp ip} \ln \left[\frac{|\omega| \bar{K}(\omega)}{1 + \lambda^2} \right]$$

$$= \pm \frac{1}{2\pi i} \left[\int_{0}^{\infty} \frac{d\omega}{-\omega \mp ip} + \int_{0}^{\infty} \frac{d\omega}{\omega \mp ip} \right] \ln \left[\frac{\omega \bar{K}(\omega)}{1 + \lambda^2} \right]$$

$$= \frac{p}{\pi} \int_{0}^{\infty} \frac{d\omega}{\omega^2 + p^2} \ln \left[\frac{\omega \bar{K}(\omega)}{1 + \lambda^2} \right] . \qquad (23)$$

So $F_+(ip)$ and $F_-(-ip)$ are real and equal. We observe that as $\omega \to 0+$, $\gamma = |\omega| = \omega$. Then, using the expansions of the Bessel functions for small argument (see Ref 2) in equation (4), we find

$$\lim_{\omega \to 0} \bar{K}(\omega) = \tfrac{1}{2}\left(1 + \lambda^2\right) .$$

Similarly, using the expansions for large argument, we find

$$\lim_{\omega \to \infty} \omega \bar{K}(\omega) = 1 + \lambda^2 ;$$

so the integral is convergent as $\omega \to \infty$ in equation (23).

Equation (6) is now used to evaluate $\bar{K}_{\pm}(\pm ip)$. We note that when $s = ip$, the appropriate branch of $(s + i\delta)^{\frac{1}{2}}$ (with positive real part) is:

$$e^{i\pi/4}(p + \delta)^{\frac{1}{2}} \to e^{i\pi/4}p^{\frac{1}{2}}$$

as $\delta \to 0$, and when $s = -ip$ the appropriate branch of $(s - i\delta)^{\frac{1}{2}}$ is

$$e^{-i\pi/4}(p + \delta)^{\frac{1}{2}} \to e^{-i\pi/4}p^{\frac{1}{2}}$$

as $\delta \to 0$: thus

$$\bar{K}_{\pm}(\pm ip) = \left(1 + \lambda^2\right)^{\frac{1}{2}} \exp\left[F_{\pm}(\pm ip)\right] \Big/ p^{\frac{1}{2}} \quad . \tag{24}$$

The function $i\hat{K}(p)$, given by equation (10), must also be written as a real function of the real variable p for computing purposes. Differentiating equations (21) and (22), putting $\nu = 2$ and $z = p$, we have

$$I_2'(-ip) = -i.J_2'(p) \tag{25}$$

$$K_2'(-ip) = \frac{\pi}{2}\left[J_2'(p) + iY_2'(p)\right] \quad . \tag{26}$$

Substituting equations (21), (22), (25) and (26) into (11) and then into (10) gives:

$$D(-ip) = \frac{\pi}{2}\left[\left(\lambda^2 - 1\right)J_2J_2' - i\left(J_2Y_2' - \lambda^2 J_2'Y_2\right)\right] \tag{27}$$

$$i\hat{K}(p) = \frac{-2\lambda^2 J_2'\left(J_2Y_2' - J_2'Y_2\right)}{\left[\left(\lambda^2 - 1\right)J_2J_2'\right]^2 + \left[J_2Y_2' - \lambda^2 J_2'Y_2\right]^2} \quad . \tag{28}$$

For brevity, we have dropped the argument p of the Bessel functions $J_2(p)$, etc on the right-hand sides. It also follows from equation (25) that in the integrand in equation (13) the factor $iI_2'(ip)$ can be replaced by $\left[-J_2'(p)\right]$.

Making use of the Wronskian relation[2]

$$J_2Y_2' - J_2'Y_2 = \frac{2}{\pi p} \quad , \tag{29}$$

equations (27) and (28) are written:

$$D(-ip) = \frac{\pi}{2}\left(\lambda^2 - 1\right)J_2\left(J_2' + iY_2'\right) - \frac{\lambda^2 i}{p} \tag{30}$$

$$i\hat{K}(p) = \frac{-2\lambda^2\left(\frac{2}{\pi p}\right)J_2'}{\left[\left(\lambda^2 - 1\right)J_2J_2'\right]^2 + \left[\left(\frac{2}{\pi p}\right) - \left(\lambda^2 - 1\right)J_2'Y_2\right]^2} \quad . \tag{31}$$

When $\lambda = 1$, they simplify to:

$$D(-ip) = -\frac{i}{p} \tag{32}$$

$$i\hat{K}(p) = -\pi p.J_2'(p) \quad . \tag{33}$$

We remark that on the regional interface $r = 1$, $x > 0$, the kinematic boundary condition, see equation (3-28) of Ref 1, requires

$$\left[\frac{\partial \psi_2}{\partial r}(r,x)\right]_{r=1} = \lambda.\left[\frac{\partial \tilde{\psi}_2}{\partial r}(r,x)\right]_{r=1} \quad . \tag{34}$$

This relation can be verified from equations (12) and (13); we find on the way that

$$2.\mathrm{Re}\,\frac{\partial}{\partial r}\frac{K_2(-ipr)}{D(-ip)}\bigg|_{r=1} = -p.i\hat{K}(p) \quad ,$$

and then both sides of equation (34) are equal to $-2\lambda x/(1 + \lambda^2) + G_2$, where

$$G_2 = -\frac{\lambda}{\pi\sqrt{2}\left(1 + \lambda^2\right)^{\frac{1}{2}}}\int_0^\infty \frac{dp}{p}.i\hat{K}(p).J_2'(p).\bar{K}_-(-ip).e^{-px}.(1 - Ap) \quad . \tag{35}$$

4 COMPUTATIONS

4.1 Zeros of J_2'

For equation (3) we need to calculate and store the positive zeros Ω_n of J_2', which is given by equation (19) with $\nu = 2$. We find the zeros by successive iteration using Newton's method: if ω is a current approximation to a zero, the next approximation is

$$\omega - \left[\frac{J_2'(\omega)}{J_2''(\omega)}\right] .$$

Using equation (19) again, we get:

$$J_2''(\omega) = \frac{1}{4}\left[J_4(\omega) - 2J_2(\omega) + J_0(\omega)\right] .$$

The Bessel functions J_2, J_3, J_4 are calculated from equation (15) with $\nu = 1,2,3$ in succession. The iteration is taken to have converged when successive iterates differ by less than 2.5×10^{-5}. At convergence, J_2'' is conveniently available for use in equation (3).

The starting guess at the first zero is $\omega = 3$. When a particular zero Ω_n has been found, mindful of the asymptotic form

$$J_2'(\omega) \sim -\left(\frac{2}{\pi\omega}\right)^{\frac{1}{2}} \sin\left(\omega - \pi - \frac{\pi}{4}\right) ,$$

we take $\omega = \Omega_n + \pi$ as the starting guess for the next zero Ω_{n+1}. The asymptotic form of J_2' follows from equation (19) and that of J_ν given in Ref 2.

To calculate typical values of $\tilde{\psi}_2$ given by equation (3) on $x = 0$ to graphical accuracy, we needed to compute as many as 400 zeros of J_2' for use in the series.

4.2 Evaluation of $\bar{K}_+(ip)$

For use (along with equation (24)) in the calculation of $\bar{K}_+(ip)$ for equation (3) we have to evaluate the integral (23) for $F_+(ip)$ at the zeros

$p = \Omega_n$. For use in equations (8), (9), (12), (13) and (14), noting that $\bar{K}_-(-ip) = \bar{K}_+(ip)$, we must evaluate equation (23) over a range of positive values of p . Leaving the origin $p = 0$ aside for the moment, we assume $p > 0$, we break the range of integration of ω into two parts $[0,p]$, $[p,\infty]$ and subtract the logarithmic singularity at $\omega = 0$ thus:

$$F_+(ip) = F_1 + F_2 + F_3$$

where

$$F_1 = \frac{p}{\pi} \int_0^p \frac{d\omega}{\omega^2 + p^2} \left[\ln \frac{\omega \bar{K}(\omega)}{1 + \lambda^2} - \ln \frac{\omega}{2} \right]$$

$$F_2 = \frac{p}{\pi} \int_0^p \frac{d\omega}{\omega^2 + p^2} \ln \frac{\omega}{2}$$

$$F_3 = \frac{p}{\pi} \int_p^\infty \frac{d\omega}{\omega^2 + p^2} \ln \frac{\omega \bar{K}(\omega)}{1 + \lambda^2}$$

F_2 , which now contains the singularity at $\omega = 0$, can be evaluated analytically (Ref 3) and the result is:

$$F_2 = \frac{1}{4} \ln\left(\frac{p}{2}\right) - \frac{G}{\pi} .$$

where G is Catalan's constant, $G = 0.9159655942 \ldots$. Making the changes of variable $\omega = pW$ for F_1 and $\omega = p/W$ for F_3 , we get:

$$F_1 = \frac{1}{\pi} \int_0^1 \frac{dW}{W^2 + 1} \ln \frac{2\bar{K}(pW)}{1 + \lambda^2}$$

$$F_3 = \frac{1}{\pi} \int_0^1 \frac{dW}{W^2 + 1} \ln \frac{(p/W)\bar{K}(p/W)}{1 + \lambda^2} .$$

The notes following equation (23) imply that the logarithms in F_1 and F_3 both go to zero as $W \to 0$. F_1 and F_3 are evaluated independently, in adaptive fashion, by the trapezium rule. The values obtained by using two and four intervals in $[0,1]$ are compared, and if they do not agree to within the specified tolerance $TOL = 10^{-5}$, the number of intervals is doubled until two successive values do agree.

As one might expect, it is found that when p is small, F_1 needs only a few subintervals, and when p is large, F_3 needs only a few subintervals so that no more work is done than is necessary, and also the program does not call for values of ω so large that the evaluation of $\bar{K}(\omega)$ fails when machine limits are encountered.

The above procedure fails for $p = 0$. However, equation (B-21) of Ref 1 quotes the behaviour of $\bar{K}_+(ip)$ for small p :

$$\bar{K}_+(ip) \to \left(\frac{1+\lambda^2}{2}\right)^{\frac{1}{2}} \quad \text{as} \quad p \to 0 \quad .$$

This trend is confirmed by inspection of the values of $\bar{K}_+$ output for small values of p . There is therefore no need to consider the integral equation (23) at $p = 0$.

For large values of p , from equation (23) $F_+(ip) = O(1/p)$ (again confirmed numerically), and so from equation (24):

$$\bar{K}_+(ip) = \left(\frac{1+\lambda^2}{p}\right)^{\frac{1}{2}}\left[1 + O\left(\frac{1}{p}\right)\right] \quad \text{as} \quad p \to \infty \quad . \tag{36}$$

4.3 Evaluation of A from equation (7)

In equations (8) and (9) we first note the behaviour of the integrands near $p = 0$ and as $p \to \infty$.

Near $p = 0$, we can introduce the series expansions of J_2 and Y_2 into equation (31) to show that $i\hat{K}(p) = O(p^2)$ and $J_2'(p) = O(p)$. Also $\bar{K}_+(ip)$ is bounded. Hence the integrands of $\bar{C}_1$ and $\bar{C}_2$ are finite except for the term $O(p^{-\frac{1}{2}})$ of $\bar{C}_2$ which however is integrable and the integral can be evaluated analytically.

We know[2] that, as $p \to \infty$:

$$\left.\begin{aligned} J_2(p) &\sim \left(\frac{2}{\pi p}\right)^{\frac{1}{2}} \cos q \\ Y_2(p) &\sim \left(\frac{2}{\pi p}\right)^{\frac{1}{2}} \sin q \end{aligned}\right\} \qquad (37)$$

where $q = p - 5\pi/4$; also

$$J_2'(p) \sim -\left(\frac{2}{\pi p}\right)^{\frac{1}{2}} \sin q$$

$$Y_2'(p) \sim \left(\frac{2}{\pi p}\right)^{\frac{1}{2}} \cos q \quad .$$

Substituting into equation (28), we find:

$$i\hat{K}(p).J_2'(p) \sim -2.\frac{\lambda^2 \sin^2 q}{\lambda^4 \sin^2 q + \cos^2 q} \quad . \qquad (38)$$

This function is periodic, non-positive and bounded, so for large P

$$\int_P^\infty \frac{dp}{p} .i\hat{K}(p).J_2'(p).\bar{K}_+(ip) = O\left(P^{-\frac{1}{2}}\right) \quad ,$$

by using equation (36). The integral equation (8) for $\bar{C}_1$ is therefore convergent as $p \to \infty$. Also, from Ref 3, the mean value of the right-hand side of equation (38) over a period π is:

$$-\frac{2}{1+\lambda^2}$$

so that, for large p , the mean value of $i\hat{K}(p).J_2'(p).\bar{K}_+(ip)$ over a period of length π is:

$$-\frac{2}{\left(1+\lambda^2\right)^{\frac{1}{2}} p^{\frac{1}{2}}} \ .$$

Hence, for large p, in the integral (9) over a period of length π the terms $O(p^{-\frac{1}{2}})$ in the square bracket cancel, the subintegral over such a period is $O(p^{-3/2})$, for sufficiently large P the integral from P to ∞ becomes a sum of such subintegrals, convergent to a value $O(P^{-\frac{1}{2}})$, and so the integral (9) for $\bar{C}_2$ is similarly convergent as $p \to \infty$.

The above argument establishes that the expressions (8) and (9) for $\bar{C}_1$ and $\bar{C}_2$ are proper. We now turn to their evaluation, considering $\bar{C}_1$ first. The approach is to evaluate the integral

$$\int_0^P \frac{dp}{p} \, .i\hat{K}(p).J_2'(p).\bar{K}_+(ip) \qquad (39)$$

for a sequence of integer values of P and to extrapolate for the limit $P \to \infty$. The range $[0,P]$ is first divided into the unit intervals $[0,1]$, $[1,2]$ ... , $[P-1,P]$. The integral over each of these unit intervals is evaluated by the trapezium rule, using up to LNPU successive bisections, but stopping when two successive estimates of the integral over the unit interval agree to within a specified tolerance TOL. LNPU and TOL are adjustable program constants. In this way, with TOL set to 10^{-5}, the estimates of the integral (39) obtained with LNPU equal to 4 and 5 were found to agree to five significant figures.

The effect of the upper limit P was studied, bearing in mind that the truncated portion from P to infinity is expected to be $O(P^{-\frac{1}{2}})$. For $\lambda = 1$, the following values of equation (39) were obtained:

P	200	400	800	1600
$\bar{C}_1$	-1.430537	-1.489004	-1.530398	-1.559720

The limit of $\bar{C}_1$ as $P \to \infty$ can be estimated by Richardson's method. Suppose we are given values of a function $f_p \equiv f(p)$ for $p = P$, $2P$ and $4P$. Assuming an error term $O(p^{-r})$, where r is an unspecified exponent, r is given by:

$$2^r = \frac{f_P - f_{2P}}{f_{2P} - f_{4P}} \ ,$$

and then

$$f_\infty = \frac{2^r f_{4P} - f_{2P}}{2^r - 1} \quad .$$

For $P = 200$ (the first three values in the Table), we obtain $2^r = 1.41287$; the last three give $2^r = 1.41200$. So we can assume as expected that $r = 1/2$. Then, extrapolating from the last two values with $2^r = 1.4142$ gives:

$$\bar{C}_1 = -1.63050 \quad . \tag{40}$$

We now turn to $\bar{C}_2$ as given by equation (9). The integral is only conditionally convergent as $p \to \infty$, and if it were evaluated in the same way as $\bar{C}_1$, we should expect slow convergence $O(P^{-\frac{1}{2}})$ as the upper limit $P \to \infty$.

From equations (37) and (38), for large p the integrand in equation (9) is asymptotically

$$\left(\frac{\lambda^2 + 1}{p}\right)^{\frac{1}{2}} \left[\frac{2}{\lambda^2 + 1} + \frac{\lambda^2(\sin 2p - 1)}{\lambda^4 \sin^2 q + \cos^2 q}\right] \quad . \tag{41}$$

The second term in the square bracket has mean value $[-2/(\lambda^2 + 1)]$, so the whole square bracket has zero mean and represents an oscillatory function with period π .

The second term in the square bracket has the following further properties: it is non-positive, and its curve touches the p-axis at $p = \pi/4 + N\pi$, where N is an integer. The function

$$\frac{2}{1 + \lambda^2}\left(\sin 2p - 1\right)$$

also has all three properties listed above, and indeed coincides with the second term when $\lambda = 1$. Therefore, for large p , the oscillatory behaviour of the complete expression (41) resembles that of:

$$\frac{2}{\left(\lambda^2 + 1\right)^{\frac{1}{2}}} \frac{\sin 2p}{p^{\frac{1}{2}}} \quad ,$$

and we expect to get better convergence as the finite outer limit $P\to\infty$ if we subtract this from the integrand in equation (9). The subtrahend can be integrated exactly[3], and the expression for $\bar{C}_2$ becomes:

$$\bar{C}_2 = \left(\frac{\pi}{1+\lambda^2}\right)^{\frac{1}{2}} + \int_0^\infty dp \left[i\hat{K}(p).J_2'(p).\bar{K}_+(ip) + \frac{2}{\left(1+\lambda^2\right)^{\frac{1}{2}} p^{\frac{1}{2}}} (1 - \sin 2p) \right] .$$

To remove the singularity $O(p^{-\frac{1}{2}})$ at the origin, we subtract another term:

$$\frac{2}{\left(1+\lambda^2\right)^{\frac{1}{2}}} \frac{e^{-p}}{p^{\frac{1}{2}}}$$

which has the same behaviour as the integrand as $p\to\infty$, and is exponentially small as $p\to\infty$. Again the subtrahend can be integrated exactly[3], and the expression for $\bar{C}_2$ becomes:

$$\bar{C}_2 = 3\left(\frac{\pi}{1+\lambda^2}\right)^{\frac{1}{2}} + \int_0^\infty dp \left[i\hat{K}(p).J_2'(p).\bar{K}_+(ip) + \frac{2}{\left(1+\lambda^2\right)^{\frac{1}{2}} p^{\frac{1}{2}}} \left(1 - \sin 2p - e^{-p}\right) \right] . \quad \ldots\ldots (42)$$

The integrand now vanishes at the lower limit, and we can again use the trapezium rule.

The integrand is still oscillatory, and so we evaluate $\bar{C}_2$ as a succession of loops of alternately positive and negative area (above and below the p-axis). The contributions from the loops are stored separately in a one-dimensional array. A loop is deemed complete, and a new loop is started, when the integrand changes sign between two integration points; the contribution to the integral from these two points is split appropriately into a part which is accumulated into the now completed loop, and another which starts the new loop. We expect that the sum of an even number of these loops will show a more consistent trend as $P\to\infty$ than the result of cutting off the integration at fixed values of P, which would correspond to cutting off random fractions of either a positive or negative loop.

To apply Richardson extrapolation to three partial sums of this alternating series, we use the loop counter L as the variable. Taking the largest loop number to be four times the smallest, which should itself be even, we stop the summation at the largest multiple of 8 loops allowed by the outer limit P . Setting P = 800 , and also putting $\lambda = 1$ which corresponds to the special case mentioned in the Introduction, we obtain the results shown in the Table:

L	126	252	504
$\bar{C}_2$	6.08846	6.14185	6.16526

These give:

$$2^r = 2.2806, \quad r = 1.189, \quad \bar{C}_2(\infty) = 6.1835 \ .$$

Had we stopped short of P = 400 , the Table would have been:

L	64	128	256
$\bar{C}_2$	6.01206	6.08995	6.14276

which would have given:

$$2^r = 1.4749, \quad r = 0.561, \quad \bar{C}_2(\infty) = 6.2540 \ .$$

Clearly Richardson extrapolation is somewhat uncertain, though r should be heading for the value 1.5 . However, a run with P = 1600 produces the following Table:

L	254	508	1016
$\bar{C}_2$	6.14231	6.16529	6.13653

$\bar{C}_2$ is not monotonic in this range, so Richardson's method fails altogether. This may be a warning that the asymptotic behaviour has not yet been reached, or it may be due to a lack of accuracy in the evaluation of $\bar{C}_2$. In either case, some caution is indicated. We propose for the amount to take the extrapolated value arising from P = 800 above: $\bar{C}_2 = 6.1835$. From equations (7) and (40), and this estimate for $\bar{C}_2$, we get a tentative value:

$$A = -0.2637 \ . \qquad (43)$$

4.4 The solution inside the pipe and inside the jet

We can now evaluate the sum (3) for $r \leqslant 1$, $x \leqslant 0$, and the integral (12) for the region inside the jet $r \leqslant 1$, $x \geqslant 0$. On the line $x = 0$, where the exponential factors are all equal to unity, the results are likely to be least accurate, but inspection of the computed results for equation (12) suggests that for the integration outer limit $P = 800$, they are accurate to at least three significant figures so that we can expect them to be adequate for graphical purposes. The summation over the first 400 zeros of J_2' in equation (3) should give at least similar accuracy, since $\Omega_{400} \doteq 400\pi \doteq 1250$.

On this crucial interface, the two solutions should agree. Fig 2(a) shows their behaviour there for $\lambda = 1$, and we can see that they do agree qualitatively, but not quantitatively; the curve for $\tilde{\psi}_2(x = 0-,r)$ (inside the pipe) lies above that for $\tilde{\psi}_2(x = 0+,r)$ (inside the jet).

An exercise was mounted to see whether the differences might be largely due to a small error in evaluating A , which is a somewhat uncertain quantity in view of the investigation reported in section 4.3. When $(-A)$ is reduced by 0.01 to the value 0.2537, a qualitatively similar picture is obtained (Fig 2b) in which the differences are reversed in sign and the curve for $x = 0-$ now lies below that for $x = 0+$. At $r = 0.8$, where the difference between the two curves is greatest, linear interpolation of the differences produces a new value

$$A = -0.25944 \qquad (44)$$

and the other values $r = 0.1(0.1)1.0$ yield consistent values of A which differ by no more than 0.0003 , except for a value (-0.25846) at $r = 0.1$, where the difference between the two curves is too small for the interpolation to be meaningful.

With A given by equation (44), the two curves for $x = 0-$ and $x = 0+$ agree as shown in Fig 3. As a further check, extra values for $r = 0.91(0.01)0.99$ are plotted and also show good agreement. The increasing gradient towards $r = 1$ is to be expected since (Ref 1) the velocity field exhibits a square-root singularity at the orifice lip.

It is disappointing that the value (44) of A required to ensure a close match of the pipe and jet solutions differs by as much as 1.6% from the best prior estimate, equation (43), of A . The difficulty appears to lie in the calculation of $\bar{C}_1$ and $\bar{C}_2$. For instance, if we reject the Richardson

extrapolation and use the values $\bar{C}_1 = -1.55972$ and $\bar{C}_2 = 6.13653$ obtained with the largest values of p (1600) and L (1016) used, we find $A = -0.2542$, which is as far above equation (44) as equation (43) is below it. The discrepancy therefore indicates that the analytic expressions given in Ref 1 are not convenient for numerical evaluation, but it does not suggest that they are in any way inconsistent.

To demonstrate the relation between the solutions inside the pipe and inside the jet, Fig 4 shows a contour map of $\tilde{\psi}_2$ in the region $-1 \leqslant x \leqslant 1$, $0 \leqslant r \leqslant 1$, with A given by equation (44); the contours vary smoothly across the common boundary $x = 0$. The contour values have been multiplied by 100 to get three significant figures in the standard plotting package[4] used. No contours appear at the top left of the Figure because the disturbance velocity is almost zero there. The contours at the bottom right have been omitted because the velocity potential varies rapidly there and we wish to concentrate attention on the interface region.

Data are supplied to the plotting routine at the nodes of the grid shown; linear interpolation is used along the grid lines, and the contours are formed from straight-line segments joining points on the grid lines. Near the orifice lip this is clearly inadequate, so the solution there has been computed at more points and plotted on a scale ten times as large in Fig 5. Again the contours cross the common boundary smoothly. The representation is still lacking in detail near the lip, so a further enlargement by a factor of ten is shown in Fig 6. Irregularities now appear near the interface at $x = 0$. However, we note that the contours in Fig 6 are approximately similar in shape, indicating that the smallest-scale flow features are now being picked up. This scale is remarkably small - the width of the region in Fig 6 is only 1% of the pipe radius. As an indication of the significance of the different scales, we note the change in direction of the equipotentials along the bottom of Figs 4 to 6. At $x = 1$, Fig 4, the equipotentials are approximately aligned with the pipe axis; at $x = 0.1$, Fig 5, they are approximately normal to the pipe axis, and at $x = 0.01$, Fig 6, they are again more nearly aligned with the axis. Along the pipe wall, $r = 1$, $x < 0$, the equipotentials are normal to the wall, in accordance with the boundary condition, wherever the scale allows their proper representation.

We note, from the relatively wide spacing of the equipotentials towards the top of Fig 4, that the disturbance caused by the external flow to the flow in the pipe has decayed to a negligible level within one pipe radius upstream of the orifice.

4.5 The solution on the jet boundary

We turn now to the solution on the jet boundary, represented in the present linearized treatment by the half-cylinder $r = 1$, $x \geqslant 0$. It was shown at the end of section 3 that the kinematic boundary condition is satisfied and that

$$\left.\frac{\partial \tilde{\psi}_2}{\partial r}\right|_{r=1} = -\frac{2x}{1+\lambda^2} + \frac{G_2}{\lambda}$$

where $$G_2 = -\frac{\lambda}{\pi\sqrt{2}\left(1+\lambda^2\right)^{\frac{1}{2}}} \int_0^\infty \frac{dp}{p} .i\hat{K}(p).J_2'(p).\bar{K}_-(-ip).e^{-px}\,(1-Ap) \quad . \qquad (35)$$

This expression is related to the jet shape, given by $F(r,\theta,x) = 0$, by the kinematic boundary condition $\nabla F.\nabla\tilde{\rho} = 0$, where

$$\tilde{\rho} = x + \varepsilon^2\,\tilde{\psi}_2(r,x)\,\cos 2\theta + O\left(\varepsilon^3\right) \quad ,$$

by equation (2), with the axially symmetric perturbation $\tilde{\psi}_0$ omitted. If F is expanded in the form

$$F(r,\theta,x) = r - 1 - \varepsilon^2\,f(x)\,\cos 2\theta + O\left(\varepsilon^3\right) \quad ,$$

the above kinematic boundary condition gives, to leading order in ε ,

$$\frac{df}{dx} = \left.\frac{\partial \tilde{\psi}_2}{\partial r}\right|_{r=1} .$$

Hence the slope of the jet surface in a meridian plane, $\theta = \text{const.}$, is given by

$$\frac{\partial r}{\partial x} = \varepsilon^2.\frac{df}{dx}.\cos 2\theta = -\frac{2\varepsilon^2\,x\,\cos 2\theta}{1+\lambda^2} + \frac{\varepsilon^2 G_2\,\cos 2\theta}{\lambda} \qquad (45)$$

to leading order in ε .

The first term on the right of equation (45) is the leading term in the expansion of the solution given in section 3.1 of Ref 1 for the development of

the jet away from the immediate neighbourhood of the orifice. When x is large enough for this term to dominate the second, equation (45) represents a flattening of the jet cross-section, increasing with distance from the orifice, produced by a lateral expansion, for θ near $\pm\pi/2$, and a fore-and-aft contraction for θ near 0 and $\pm\pi$.

Considering now the second term in equation (45), we note first that it is positive for $\lambda = 1$, because the integrand in equation (35) is non-positive and not identically zero for p real and positive. The product $i\hat{K}(p)J_2'(p) \leqslant 0$ and only vanishes at the zeros of J_2' by equation (33). $\bar{K}_-(ip) > 0$ by equation (24) since $F_-(-ip)$ is real by equation (23). The exponential is positive, and $(1-Ap)$ is positive because A is negative. The two terms on the right of equation (45) are therefore opposed, and we shall see that the second term is dominant near the orifice.

The integral in equation (35) closely resembles that in equation (12), so G_2 can be evaluated by a modified version of the code written to deal with equation (12), provided that the integral is convergent. In fact, the change from J_2 in equation (12) to J_2' in equation (35) is unimportant, but the extra factor p makes equation (35) divergent at infinity for $x = 0$. Numerical evaluation is therefore restricted to $x > 0$. For $\lambda = 1$, the variation of G_2 with x is shown in Fig 7. We note first that it decays to zero as x increases, so that equation (45) is consistent with the form found[1] for the jet away from the orifice. The rapid decay is consistent with the proportionality to x^{-3} predicted by equation (3-39) of Ref 1 for the asymptotic behaviour as $x \to \infty$. The numerical solution provides the further information that, by $x = 1$, *ie* half a diameter from the orifice, the second term on the right of equation (45) is only 1.35% of the first.

On the other hand, as x tends to zero G_2 appears to increase without limit, as would be expected from the comment above about the divergence of the integral in equation (35). Hence, near the orifice the second term in equation (45) dominates and $\partial r/\partial x$ therefore changes sign on $r = 1$ as x increases from zero. The interpretation of this is discussed later.

The calculated behaviour of G_2 as the orifice lip, $r = 1$, $x = 0$, is approached can be related to the analysis of Ref 1 in the following way. At the end of Appendix B of Ref 1, the asymptotic expression is obtained:

$$\frac{\partial \tilde{\psi}_2}{\partial r} \sim -\left(\frac{2}{\pi}\right)^{\frac{1}{2}} \frac{A}{1+\lambda^2} x^{-\frac{1}{2}} \quad , \tag{46}$$

valid for $r = 1-$ as $x \to 0+$. Hence, for $\lambda = 1$, with A given by equation (44)

$$G_2 \sim 0.1035\, x^{-\frac{1}{2}} \quad .$$

Calculated values of G_2 are used in the Table below:

x	0.1	0.05	0.02	0.01
G_2	0.2215	0.3736	0.6661	0.9801
$x^{\frac{1}{2}} G_2$	0.0700	0.0835	0.0942	0.0980

It is apparent that the value 0.1035 from equation (46) is a plausible extrapolation of the calculated values of $x^{\frac{1}{2}} G_2$.

4.6 Singular behaviour at lip

Further analysis shows that the solution obtained in Ref 1 is two-dimensional sufficiently near the lip of the pipe, as would be expected. The singular behaviour is that of the planar incompressible potential flow round a semi-infinite plate, in which the velocity potential is proportional to $\rho^{\frac{1}{2}} \sin(\chi/2)$, where $\rho e^{i\chi}$ is the complex coordinate relative to the plate edge and $-\pi < \chi < \pi$, so that here $\rho e^{i\chi} = x + i(r-1)$. The streamlines of this flow are sketched in Fig 8a. The constant of proportionality for the flow inside the pipe and jet follows from equation (46), so that

$$\tilde{\psi}_2 \sim -\left(\frac{2}{\pi}\right)^{\frac{1}{2}} \frac{2A}{1+\lambda^2} \rho^{\frac{1}{2}} \sin\frac{\chi}{2} \quad . \tag{47}$$

On the inside of the pipe, $\chi = -\pi$ and $\rho = -x$, so

$$\tilde{\psi}_2 \sim \left(\frac{2}{\pi}\right)^{\frac{1}{2}} \frac{2A}{1+\lambda^2} (-x)^{\frac{1}{2}} \quad . \tag{48}$$

This singular term makes no contribution to the velocity potential on the jet boundary $\chi = 0$, but a glance at Fig 6 shows that $\tilde{\psi}_2$ varies noticeably along this line, even close to the lip. We therefore write, as an approximation to

$\tilde{\psi}_2(1,x)$ for $\lambda = 1$ and for x near zero, the function $\tilde{\psi}_{2A}$, where

$$100\ \tilde{\psi}_{2A} = 2.0728 - 0.4893\ (100\ x) - \begin{cases} 0 & , x \geqslant 0 \\ 2.0700\ (-100\ x)^{\frac{1}{2}} & , x \leqslant 0 \end{cases} . \qquad (49)$$

In this expression, the constant and linear terms are a fit to values of $\tilde{\psi}_2$ computed for $r = 1$ and $0 \leqslant 100\ x \leqslant 1$, and the coefficient of the fractional power follows from equation (48) with $\lambda = 1$ and A given by equation (44).

Fig 9 shows a plot of the asymptotic expression (49) with computed values superimposed, for $-1 \leqslant 100\ x \leqslant 1$. It is not surprising that the regular part of the solution is well represented by the two regular terms in equation (48) as shown by the agreement for $x > 0$, since the range of values of x is so small. The agreement for $x < 0$ is less good, but supports the validity of equation (47) and the determination of A for $\lambda = 1$. Outside of the pipe and jet, an expression like equation (46) but with a factor λ on the right-hand side is quoted in Ref 1 for ψ_2, so a similar treatment would be possible if we were to evaluate the expression (13) and (14).

We have not calculated the variation of A with λ. However, a simple argument shows that A is never zero. By equation (7), if A is to vanish $\bar{C}_1$ must vanish; by equation (8) if $\bar{C}_1$ is to vanish the integrand of the integral on the right must change sign; but by equations (23) and (24) $\bar{K}_+(ip)$ is never negative, and by equation (31) $i\hat{K}(p)J_2'(p)$ is never positive, so the integrand is never positive. Therefore A is non-zero and the flow singularity exists for all values of λ. We recall its dependence on θ, the angular position round the lip. Omitting $\tilde{\psi}_0$ from equation (2), we have the velocity potential inside the pipe and jet, close to $x = 0$:

$$\tilde{\phi} = x + \varepsilon^2\ \tilde{\psi}_2(r,x)\ \cos 2\theta + O\left(\varepsilon^3\right) . \qquad (50)$$

The singular behaviour therefore vanishes (at least to this order) for $\theta = \pm \pi/4$, $\pm 3\pi/4$, but not elsewhere. A similar singular behaviour appears at the sharp trailing-edge of a flat-plate aerofoil at incidence in the absence of circulation; however, for the jet no eigensolution corresponding to the circulatory flow about the aerofoil seems to be available to allow a Kutta condition to be satisfied at the lip.

It appears therefore that the singularity is an essential feature of the present treatment. Since this treatment is based on a linearization, it represents a local inconsistency therein: disturbances assumed to be small emerge as being unbounded. Moreover, the failure to satisfy a Kutta condition implies that the solution is unacceptable, at least locally, as a limiting form of a viscous flow in the limit of infinite Reynolds number. The view taken in Ref 1 is that the breakdown of the solution at the lip is a local breakdown of the linearization assumption, and that the difficulty can be resolved by the solution of a non-linear problem near the lip. It is expected that a numerical solution would be required and it is not clear that such a solution would exist. Indeed, Küchemann[5,6] suggests that the inviscid representation of the mixing of uniform streams at different total pressures downstream of a splitter plate involves a convoluted vortex sheet, as sketched on the right in Fig 10, in an essentially time-dependent process. If that were so, it would have important consequences for understanding and calculating the initial formation of the jet in cross-flow.

The resolution of this difficulty requires further effort. For the moment, we confine ourselves to an attempt to interpret the existing solution in as meaningful a way as possible. From equation (50) we have, for the circumferential component of velocity inside the pipe and jet, near the orifice:

$$\frac{1}{r}\frac{\partial \tilde{\phi}}{\partial \theta} = -\frac{2}{r}\varepsilon^2 \tilde{\psi}_2(r,x) \sin 2\theta + O\left(\varepsilon^3\right) \quad . \tag{51}$$

Hence, particles lying in the two planes defined by $\theta = 0$ (and $\pm\pi$) and by $\theta = \pm \pi/2$ remain in those planes and it is instructive to sketch the streamlines they follow. We concentrate on the neighbourhood of the lip and the case $\lambda = 1$, for which $\tilde{\psi}_{2A}$, as given by equation (49), is an adequate representation of $\tilde{\psi}_2(1,x)$, and consider $\theta = \pi/2$. Then, writing $B = 0.1035$, by equations (49) and (50)

$$\left.\frac{\partial \tilde{\phi}}{\partial x}\right|_{r=1,\theta=\pi/2,x<0} \doteq 1 - \varepsilon^2\left[-0.4893 + B(-x)^{-\frac{1}{2}}\right] \quad , \tag{52}$$

inside the pipe. This expression vanishes at

$$x = x_s \doteq -B^2\varepsilon^4 \quad ,$$

for $\epsilon << 1$. Since the circumferential and radial components vanish by equation (51) and the boundary condition, the point $x = x_s$, $r = 1-$, $\theta = \pi/2$ is a stagnation point of the flow. We note that it lies extremely close to the lip. Downstream of the lip

$$\left.\frac{\partial\tilde{\phi}}{\partial r}\right|_{r=1,\theta=\pi/2,x>0} = -\epsilon^2 \left.\frac{\partial\tilde{\psi}_2}{\partial r}\right|_{r=1,x>0} . \qquad (53)$$

The contribution G_2 to the derivative on the right is plotted in Fig 7. The flow is therefore inward across the line $r = 1$ on a scale larger than x_s , and we are led to sketch a streamline pattern in the vicinity of the lip as in Fig 8b. On a smaller scale the pattern of Fig 8a appears, and on a larger scale the global flow in this, the lateral plane, is outwards, as discussed in Ref 1. It must be remembered that the present treatment is based on the assumption that the two streams, of different total pressure, are separated by the stream surface through the lip, supposed not to depart too far from the surface $r = 1$, $x \geqslant 0$. The flow of ambient fluid round the lip, even on a very small scale, as drawn in Fig 8b, represents a significant violation of that assumption.

A slightly more consistent pattern is achieved by modifying the behaviour at the stagnation point, as shown in Fig 8c. If the streamline forming the boundary between the two streams leaves the pipe wall tangentially, the ambient stream can stagnate at a pressure below the stagnation pressure of the jet. Although we have not examined the flow outside the pipe and jet in the same detail, it is to be expected that a stagnation point will occur on the outside of the pipe at $\theta = 0$ (and π), in the plane of the cross-flow, at a distance from the lip similar to $-x_s$. In this case, illustrated in Fig 8d, the jet fluid, at total pressure above ambient, flows outward round the lip and the ambient flow stagnates. On the large scale, the flow in this plane is inwards, as discussed in Ref 1.

The streamline pattern of Fig 8c is similar to that on the left of Fig 10, which is taken from Küchemann[5,6]. In a discussion of various ways in which flows involving edge singularities can be modified in order to satisfy a Kutta condition, he suggests that the unrealistic jet flow on the left might be modified to produce the flow on the right. This involves shedding a train of vortices, represented by a rolled-up vortex sheet, from the lip, in an essentially unsteady flow. It is not clear that the downstream growth of the vortices shown in Fig 10 is related to the satisfaction of the Kutta condition. As explained in Ref 7,

the growth conforms with the observed growth in the overall thickness of the shear layer and would require a further mechanism to allow the vortices to grow in strength as they are convected downstream.

We now look at the streamline pattern on the inside of the pipe just inside the lip, *ie* on the scale of x_s .

On the inside of the pipe, equation (50), with the approximation (49) for $\tilde{\psi}_2$, provides the velocity components which define the streamlines. The pattern which emerges is established in the Appendix and illustrated in Fig 11, in terms of a stretched coordinate, $\xi = -x/\delta^2$, where $\delta = B\varepsilon^2$. Fig 11a shows the pattern of the stretched streamlines in the limit of $\delta \to 0$, and Fig 11c shows it for an unrealistically large value $\delta \doteq 0.4$. The similarity of these pictures demonstrates that the pattern of stretched streamlines is almost independent of δ for the small values of δ to which the present treatment applies.

Assuming the behaviour of the flow on the outside of the pipe is qualitatively the same, we can sketch the surface streamlines very near the lip as in Fig 12. Here the pipe has first been cut along the windward generator, $\theta = \pm\pi$, then unrolled flat, and then unfolded about the lip, $x = 0$, to show the internal and external flows together. The streamlines run smoothly round the lip, the two flows colliding along a curve composed of elements similar to the streamline NS in Fig 11c. This curve has the behaviour of a three-dimensional separation line, as specified by Lighthill[8], each element of it starting at a saddle point of separation at $-x = \delta^2$, $\theta = 0$, $\pm\pi/2$, $\pm\pi$, and ending at a nodal point of separation at $x = 0$, $\theta = \pm\pi/4$, $\pm 3\pi/4$. It is, of course, a surface streamline of an inviscid flow, not a limiting streamline of a viscous flow, but continuity still requires that the three-dimensional flow leaves the surface in its neighbourhood. It thus takes over the role of the lip itself in the absence of a Kutta condition. We must remember that the scale of this flow is extremely small and that it arises from a solution which is not consistent on this small scale.

Finally, to obtain some idea of the flow in the pipe transverse to its axis we may consider the component of the velocity in such a transverse plane as defining a 'secondary flow' and sketch the 'streamlines' of this 'flow'. We must remember that they are not, of course, actual streamlines, nor even the projections of actual streamlines. The radial and circumferential velocity components are given, to leading order, by using equation (50):

$$V_r = \frac{\partial \tilde{\phi}}{\partial r} = \varepsilon^2 \frac{\partial \tilde{\psi}_2}{\partial r} \cos 2\theta$$

$$V_\theta = \frac{1}{r}\frac{\partial \tilde{\phi}}{\partial \theta} = -\frac{2\varepsilon^2}{r}\tilde{\psi}_2 \sin 2\theta \ ,$$

and so the equation governing the 'streamlines' is

$$r\frac{d\theta}{dr} = \frac{V_\theta}{V_r} = -2 \tan 2\theta . \tilde{\psi}_2 \Big/ \left(r \frac{\partial \tilde{\psi}_2}{\partial r} \right) .$$

The essential properties of $\tilde{\psi}_2(x,r)$, for $x \doteq -0.1$, may be deduced from Figs 4 and 5, *viz*, $\tilde{\psi}_2$ is negative, and

$$\frac{\partial \tilde{\psi}_2}{\partial r} < 0 \quad \text{for} \quad 0 < r < r_0$$

$$= 0 \quad \text{for} \quad r = 0 \ , \ r_0 \ \text{and} \ 1$$

$$> 0 \quad \text{for} \quad r_0 < r < 1 \ ,$$

where $r_0 \doteq 0.75$. These properties, together with a slightly more detailed examination of the relative magnitudes of $\tilde{\psi}_2$ and its derivative near $r = r_0$, are enough to establish the 'streamline' pattern shown in Fig 13. This indicates that the secondary flow takes fluid from the neighbourhood of the plane of fore-and-aft symmetry to the sides of the jet.

5 CONCLUSIONS

(1) Ref 1 presents analytical results for the flow of an inviscid incompressible jet emerging from a circular pipe into a weak cross-flow. In particular, expressions in the form of infinite series or integrals are provided for the velocity potential in the four regions: inside the pipe, inside the jet and outside both, upstream and downstream of the orifice plane. These expressions are so involved that we are unable to verify analytically the continuity of the pipe and jet solutions across the orifice. Careful numerical evaluations have now verified the continuity of these solutions for the case in which the external velocity component parallel to the pipe is equal to the pipe velocity ($\lambda = 1$). Confidence in the solution obtained in Ref 1 is thereby increased.

TM Aero 2137

(2) Ref 1 showed that disturbances to the flow in the pipe decay exponentially upstream of the orifice. The numerical solution shows that the decay is virtually complete within one pipe radius.

(3) The influence of the orifice on the jet deformation decays only algebraically, according to Ref 1. However, its influence is down to 1.4% of the total deformation within one pipe radius downstream of the orifice.

(4) The expressions given in Ref 1 are inconvenient for numerical evaluation.

(5) In Ref 1, it is shown that the solution obtained fails to satisfy a Kutta condition of smooth outflow at the pipe lip whenever the quantity A is non-zero. We show that A is never zero and that for the case $\lambda = 1$ referred to above it is large enough to affect the solution significantly.

(6) Consequently, the flow near the pipe lip should resemble the two-dimensional potential flow round the edge of a semi-infinite flat plate. It emerges that this flow behaviour occurs on an extremely small scale, and that it is embedded within a markedly three-dimensional flow pattern.

(7) If there is no steady solution satisfying a Kutta condition, a significant source of unsteadiness in real flows at high Reynolds number is apparent. It is therefore important to attempt to resolve the breakdown of the linearized approach by examining the problem near the lip on a smaller scale, as suggested in Ref 1.

Appendix

STREAMLINES ON THE PIPE SURFACE JUST INSIDE THE LIP

The velocity potential $\tilde{\phi}$ inside the pipe close to $x = 0$ is given by equation (50) and, introducing the numerical approximation equation (49) to $\tilde{\psi}_2$ we obtain

$$\tilde{\phi} = x + \varepsilon^2\left(0.02073 - 0.4893\, x - 0.2070(-x)^{\frac{1}{2}}\right)\cos 2\theta \quad , \tag{A-1}$$

to order ε^2 . Hence the dominant terms, for small x and small ε , in the axial and circumferential velocity components are:

$$\left.\begin{aligned} \partial\tilde{\phi}/\partial x &= 1 + B\varepsilon^2(-x)^{-\frac{1}{2}}\cos 2\theta \\ \partial\tilde{\phi}/r\partial\theta &= \partial\tilde{\phi}/\partial\theta = -0.4\, B\varepsilon^2 \sin 2\theta \quad , \end{aligned}\right\} \tag{A-2}$$

where $B \doteq 0.1035$, as in section 4.6. The circumferential component is everywhere small, so the streamlines are nearly aligned with the pipe axis unless the axial component is also small. The axial component can only be small if $\cos 2\theta \leqslant 0$, *ie*, $\pi/4 \leqslant |\theta| \leqslant 3\pi/4$. It is sufficient to consider the interval $\pi/4 \leqslant \theta \leqslant \pi/2$, since the streamlines in the other θ-intervals $(\pi/2\ ,\ 3\pi/4)$ and $(-3\pi/4\ ,\ -\pi/4)$ of interest follow from considerations of symmetry.

For brevity we introduce a small quantity

$$\delta = B\varepsilon^2 \quad ; \tag{A-3}$$

and, to work on an appropriate length scale, we introduce

$$\xi = -x/\delta^2 \quad , \tag{A-4}$$

noting that $\xi \geqslant 0$ in the pipe. Then the velocity components are

$$\left.\begin{aligned} \partial\tilde{\phi}/\partial x &= 1 + \xi^{-\frac{1}{2}}\cos 2\theta \\ \partial\tilde{\phi}/\partial\theta &= -0.4\,\delta \sin 2\theta \quad , \end{aligned}\right\} \tag{A-5}$$

while the streamlines satisfy the differential equation

$$\frac{d\theta}{dx} = \frac{\partial\tilde{\phi}/\partial\theta}{\partial\tilde{\phi}/\partial x} \quad . \tag{A-6}$$

Hence, along a streamline,

$$\frac{d\theta}{d\xi} = -\delta^2 \frac{d\theta}{dx} = \frac{0.4\,\xi^{\frac{1}{2}}\,\delta^3 \sin 2\theta}{\xi^{\frac{1}{2}} + \cos 2\theta} \quad , \tag{A-7}$$

and we can regard this equation as defining 'stretched streamlines' in the (θ,ξ) plane.

In the (θ,ξ) plane we can easily find the stretched streamlines for the limiting case $\delta = 0$, even though we cannot return to the physical (θ,x) space for $\delta = 0$. We recall that θ lies in the interval $[\pi/4 , \pi/2]$, so $\sin 2\theta \geqslant 0$ and $\cos 2\theta \leqslant 0$, and that $\delta \geqslant 0$. Then the numerator of the right-hand side of equation (A-7) tends to zero through positive values as $\delta \to 0$, while the denominator is negative for $\xi^{\frac{1}{2}} < -\cos 2\theta$, vanishes for $\xi^{\frac{1}{2}} = -\cos 2\theta$, and is positive for $\xi^{\frac{1}{2}} > -\cos 2\theta$. The stretched streamlines are therefore the straight lines of constant θ , on which $d\theta/d\xi$ is zero, together with the curve $\xi = \cos^2 2\theta$, on which the right-hand side of equation (A-7) is indeterminate. These lines are drawn in Fig 11a, with arrows indicating the direction of flow which follows from equations (A-5). It is to be expected that the stretched streamlines for δ non-zero, but small compared with unity, will resemble those of Fig 11a.

We now seek more definite information about the streamlines for $0 < \delta \ll 1$. It is helpful to locate and identify singular points of streamline patterns, indicated by indeterminacy of the expression for the streamline slope, and usually associated with stagnation of the flow. Inspection of equation (A-7) shows the right-hand side becomes indeterminate for $\theta = \pi/2$, $\xi = 1$ and for $\theta = \pi/4$, $\xi = 0$. Further consideration shows there are no other singular points. Reference to equation (A-5) shows that the first of these is a stagnation point, with both velocity components in the surface of the pipe vanishing. Moreover, if we expand about this point, writing $\theta = \pi/2 - \bar{\theta}$, $\xi = 1 - \bar{\xi}$, with $\bar{\theta},\bar{\xi}$ small and of the same order, we find that $d\bar{\theta}/d\bar{\xi} \sim -1.6\,\delta^3\,\bar{\theta}/\bar{\xi}$.

From first principles, or by consulting standard texts, it follows that the point $\theta = \pi/2$, $\xi = 1$ is a saddle point, at which the streamline directions are along $\bar{\theta} = 0$, $\theta = \pi/2$ and along $\bar{\xi} = 0$, $\xi = 1$. It is labelled S in Fig 11c. The second singular point at $\theta = \pi/4$, $\xi = 0$, labelled N in Fig 11c, is not a stagnation point, since $\partial\tilde{\phi}/\partial\theta$ is negative there. Expansion about the point suggests that the local behaviour is essentially non-linear. With $\theta = \pi/4 + \bar{\bar{\theta}}$, where $\bar{\bar{\theta}}$, $\xi << 1$, equation (A-7) gives

$$\frac{d\bar{\bar{\theta}}}{d\xi} \sim \frac{0.4\ \delta^3\ \xi^{\frac{1}{2}}}{\xi^{\frac{1}{2}} - 2\bar{\bar{\theta}}} \quad . \tag{A-8}$$

From this equation we find that there are again just two directions along which stretched streamlines reach the point N , namely, along $\xi = 0$, when $\xi \sim 4\bar{\bar{\theta}}^2$, and along $\bar{\bar{\theta}} = 0.4\ \delta^3\xi$, when $\xi >> 4\bar{\bar{\theta}}^2$. The point resembles a node, but equation (A-8) does not seem to be equivalent to a linear system, so the standard classification of singular points may not be applicable.

We now find a particular solution of equation (A-7), valid for $\delta << 1$, which connects the two singular points S and N . We are guided by the solution $\xi = \cos^2 2\theta$ for $\delta = 0$ shown in Fig 11a and repeated as the broken line in Fig 11c. For convenience, let

$$\cos 2\theta = -\eta\ ,\ \eta \geqslant 0\ ,$$

so that equation (A-7) becomes

$$\frac{d\xi}{d\eta} = \frac{2\left(1 - \eta\ \xi^{-\frac{1}{2}}\right)}{\alpha\left(1 - \eta^2\right)} \quad , \tag{A-9}$$

where α is another small parameter defined by

$$\alpha = 1.6\ \delta^3 = 1.6\ B^3\ \varepsilon^6\ ,\ B \doteq 0.1035 \quad . \tag{A-10}$$

Then, if we assume an expression of the form

$$\xi = \eta^2\left[1 + \alpha\eta\left(1 - \eta^2\right)\left(f_0(\eta) + \alpha\eta f_1(\eta) + \alpha^2\eta^2 f_2(\eta) + \ldots\right)\right] \quad , \tag{A-11}$$

we have

$$\eta\xi^{-\frac{1}{2}} = 1 - \tfrac{1}{2}\alpha\eta\left(1-\eta^2\right)\left(f_0 + \alpha\eta f_1 + \alpha^2\eta^2 f_2 + \ldots\right)$$

$$+ 3/8\,\alpha^2\eta^2\left(1-\eta^2\right)^2\left(f_0 + \alpha\eta f_1 + \ldots\right)^2 - 5/16\,\alpha^3\eta^3\left(1-\eta^2\right)^3\left(f_0 + \ldots\right)^3 + \ldots$$

and

$$d\xi/d\eta = 2\eta + \alpha\eta^2\left(3-5\eta^2\right)\left(f_0 + \alpha\eta f_1 + \ldots\right)$$

$$+ \alpha\eta^3\left(1-\eta^2\right)\left(f_0' + \alpha\eta f_1' + \ldots\right) + \alpha\eta^3\left(1-\eta^2\right)\left(\alpha f_1 + \ldots\right) .$$

Hence, on introducing these expressions into equation (A-9) and equating the coefficients of like powers of α on the two sides of the equation, we find:

$$\alpha^0: \; f_0 = 2$$

$$\eta^2\alpha^1: \; \left(3-5\eta^2\right)f_0 + \eta\left(1-\eta^2\right)f_0' = f_1 - 3/4\left(1-\eta^2\right)f_0^2$$

$$\eta^3\alpha^2: \; \left(3-5\eta^2\right)f_1 + \eta\left(1-\eta^2\right)f_1' + \left(1-\eta^2\right)f_1 = f_2 - 3/2\left(1-\eta^2\right)f_0 f_1$$

$$+ 5/8\left(1-\eta^2\right)^2 f_0^3 .$$

From the structure of this sequence of equations it appears that the functions f_0, f_1, f_2, ... can be found sequentially and explicitly, and that each is a polynomial in η^2. In particular

$$f_1 = 9 - 13\eta^2$$

$$f_2 = 2\left(29 - 94\eta^2 + 69\eta^4\right) .$$

It is not obvious that equation (A-11) is a convergent series in α for all η. We therefore regard it as an asymptotic expression and re-write it in the form

$$\xi = \eta^2 + \alpha F_1(\eta) + \alpha^2 F_2(\eta) + \alpha^3 F_3(\eta) + \ldots \qquad (A\text{-}12)$$

where $F_1 = 2\eta^3\left(1 - \eta^2\right)$

$$F_2 = \eta^4\left(1 - \eta^2\right)\left(9 - 13\eta^2\right)$$

$$F_3 = 2\eta^5\left(1 - \eta^2\right)\left(29 - 94\eta^2 + 69\eta^4\right) .$$

The behaviour of these functions is illustrated in Fig 11b. Remembering that the entire treatment depends on ε being small compared with unity, we regard $\varepsilon = 0.5$ as the largest eligible value. Then, by equation (A-10), $\alpha \doteq 3 \times 10^{-5}$ is the largest eligible value of α, so the first two terms in equation (A-12) are sufficient for present purposes.

In a graphical representation of the stretched streamlines, this particular solution will be indistinguishable from the curve $\xi = \cos^2 2\theta$ if α is as small as 3×10^{-5}. In order to illustrate the structure of the stretched streamlines, an unrealistically large value of 0.1 is assigned to α, leading to the particular streamline shown by the full line connecting S and N in Fig 11c. We can then sketch the stretched streamlines between this particular streamline and the lip as shown in the Figure, noting that they leave the lip with infinite slope, that $\partial\tilde{\phi}/\partial\theta$ is negative, that $\partial\tilde{\phi}/\partial x$ and therefore $\partial\tilde{\phi}/\partial\xi$ vanish on the broken line, and that they cannot cross the particular streamline. The stretched streamlines upstream of the particular streamline can be added, on the basis that $\partial\tilde{\phi}/\partial x$ is positive and therefore $\partial\tilde{\phi}/\partial\xi$ is negative, that $\partial\tilde{\phi}/\partial\theta$ is negative and much smaller in absolute value than $\partial\tilde{\phi}/\partial\xi$ except close to the particular streamline, and that they cannot cross the particular streamline. The sketch in Fig 11c is thus completed.

LIST OF SYMBOLS

a	pipe radius
A	$\bar{C}_1/\bar{C}_2$ ($\doteq 0.26$ for $\lambda = 1$)
B	constant ($\doteq 0.10$ for $\lambda = 1$)
$\bar{C}_1, \bar{C}_2$	constants, see equations (8) and (9)
D	see equation (11)
F_+, F_-	see equation (5)
G_2	see equation (35)
I_ν	modified Bessel function of first kind and integral order ν
J_ν	Bessel function of first kind and integral order ν
K_ν	modified Bessel function of second kind and integral order ν
$\bar{K}$	see equation (4)
$\bar{K}_+$, $\bar{K}_-$	see equation (6)
$\hat{K}$	see equation (10)
p	real variable
q	$p - 5\pi/4$
r	distance from pipe axis, referred to pipe radius (also exponent in Richardson's method)
s	complex variable
$\bar{x}$	distance downstream of orifice plane
x	$\bar{x}/a$
x_s	value of x at stagnation point inside pipe
Y_ν	Bessel function of second kind and integral order ν
α	small parameter ($1.6\ \delta^3$)
δ	$B\epsilon^2$ (also arbitrary small quantity)
ϵ	ratio of cross-flow speed to jet speed
θ	angular coordinate about pipe axis, measured from leeward generator
λ	ratio of co-flow speed to jet speed
ξ	stretched axial coordinate, $-x/\delta^2$

LIST OF SYMBOLS (concluded)

$\phi(x,r,\theta)$	velocity potential outside pipe and jet
$\tilde{\phi}(x,r,\theta)$	velocity potential inside pipe and inside jet
$\psi_0(r,x)$	axisymmetric part of ϕ
$\tilde{\psi}_0(r,x)$	axisymmetric part of $\tilde{\phi}$
$\psi_2(r,x)$	non-axisymmetric part of ϕ , to order ε^2
$\tilde{\psi}_2(r,x)$	non-axisymmetric part of $\tilde{\phi}$, to order ε^2
$\tilde{\psi}_{2A}(x)$	numerical fit to $\tilde{\psi}_2(1,x)$, see equation (49)
ω	complex variable
Ω_n	n^{th} positive zero of J_2'

REFERENCES

No.	Author	Title, etc
1	D.J. Needham N. Riley J.H.B. Smith	A jet in cross-flow. *Journal of Fluid Mechanics*, 188, pp 159-184 (1988)
2	N.W. McLachlan	Bessel functions for engineers. Clarendon Press, Oxford, 2nd Ed., p 191 ff., (1955)
3	-	Table of integrals. Ministry of Supply TIB/MISC/873 (1944)
4	D. Catherall	A description of some plotting programs for analyzing results from two-dimensional flow solvers. RAE Technical Memorandum Aero 2104 (1987)
5	D. Küchemann	On some possible ways of fulfilling the Kutta condition. *Schiffstechnik*, 20, 102, pp 72-73 (1973)
6	D. Küchemann	The aerodynamic design of aircraft. Pergamon, p 48 (1978)
7	Susan M. Damms D. Küchemann	On a vortex-sheet model for the mixing between two parallel streams. *Proc. Roy. Soc.*, *A*, 339, pp 451-461 (1974) RAE Technical Report 72139 (1972)
8	M.J. Lighthill	Laminar boundary layers. Ed. L. Rosenhead, OUP, p 78 (1963)

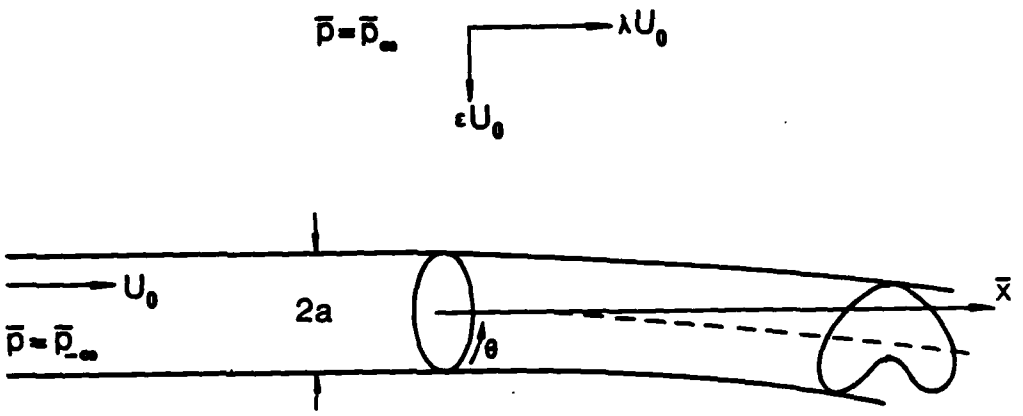

Fig 1 Definition sketch of configuration

Fig 2

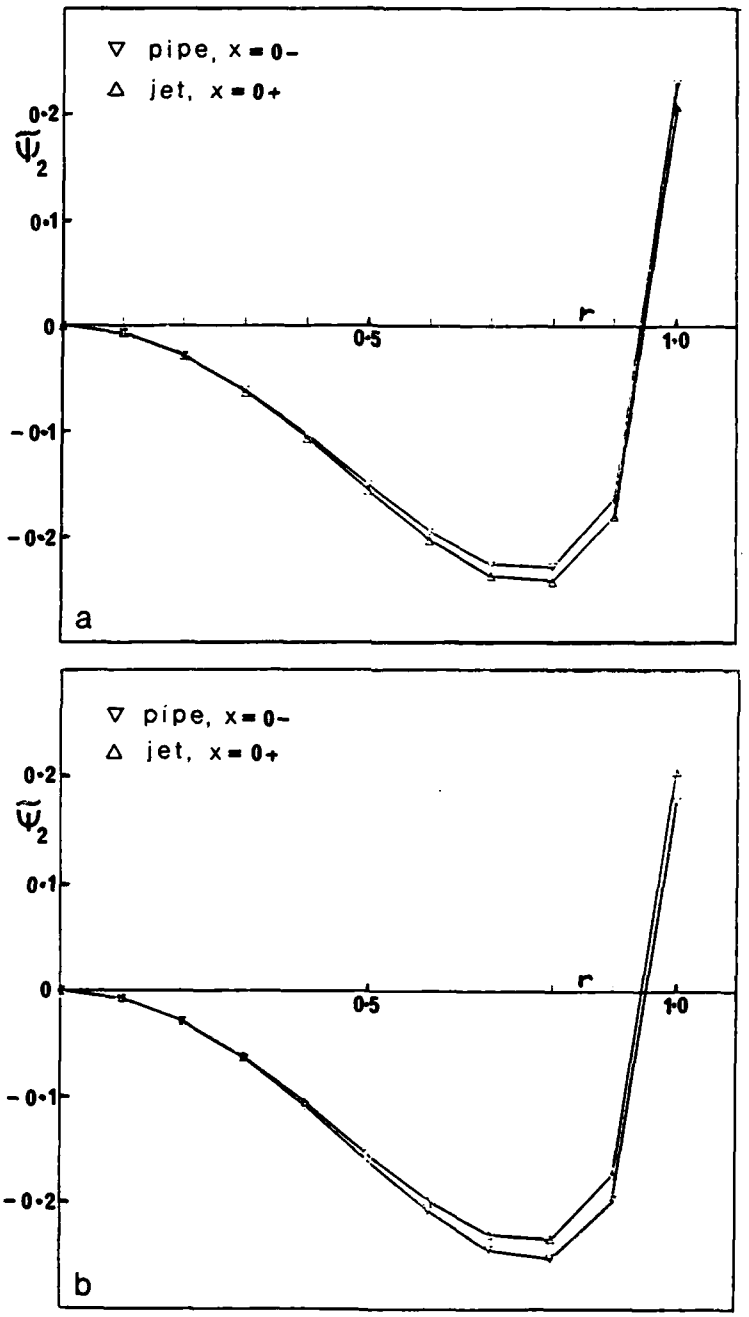

Fig 2 $\tilde{\psi}_2(r, x = 0\pm)$ computed with trial values of A = -0.2637(a) and -0.2537(b) for $\lambda = 1$

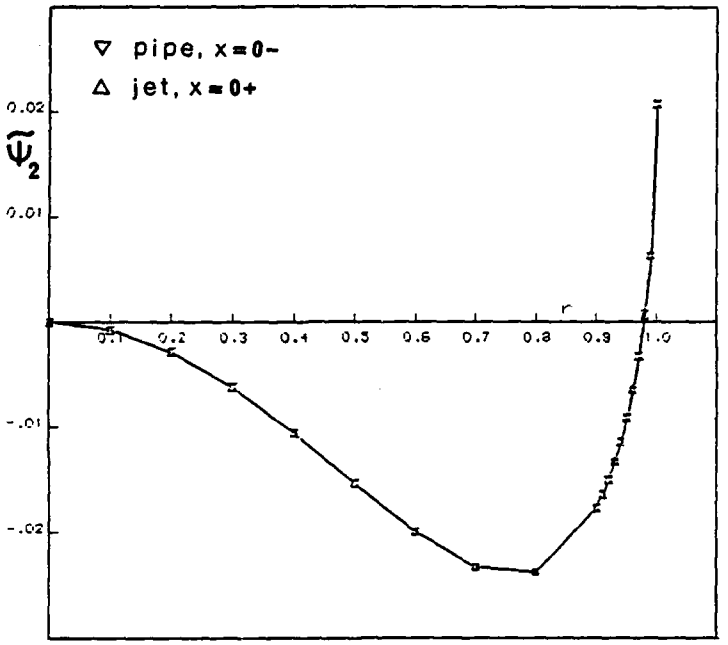

Fig 3 $\tilde{\psi}_2(r, x = 0\pm)$ computed with A = -0.25944

Fig 4

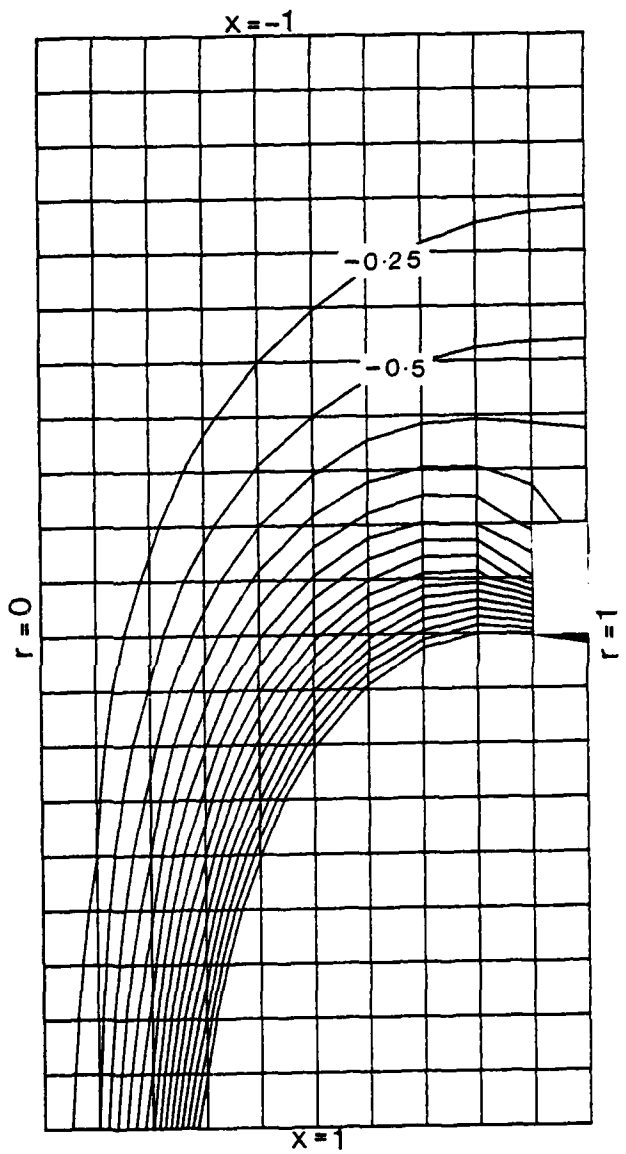

Fig 4 Contours of $100\tilde{\psi}_2$ inside pipe and jet for $\lambda = 1$, at values -4(0.25)-0.25

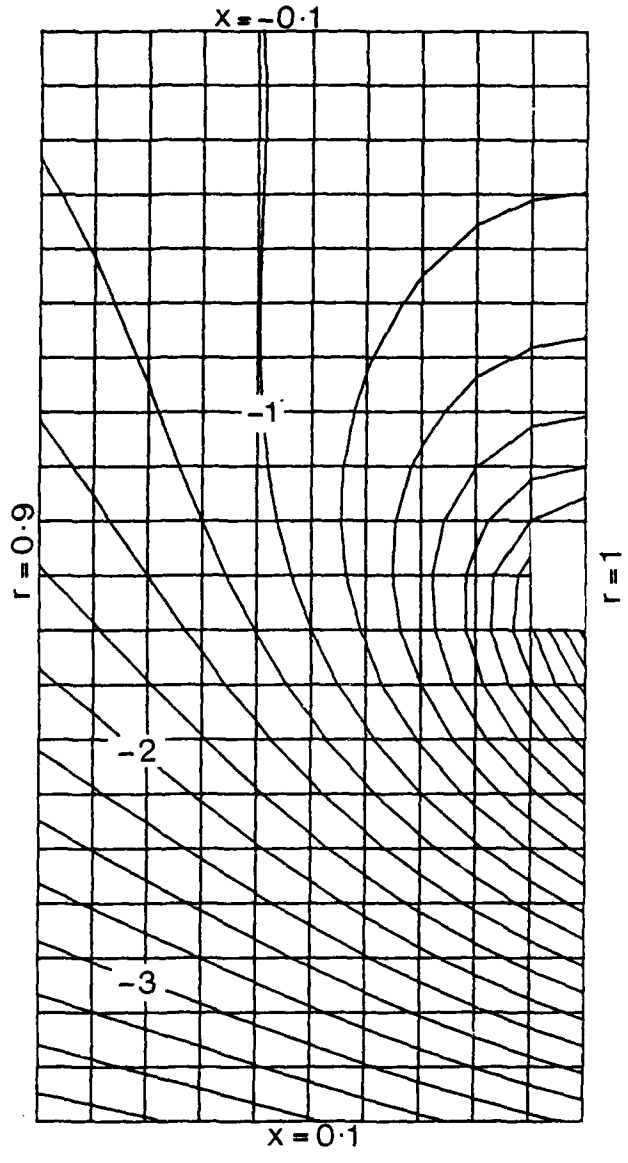

Fig 5 As Fig 4, detail near lip, -3.75(0.25)1.50

Fig 6

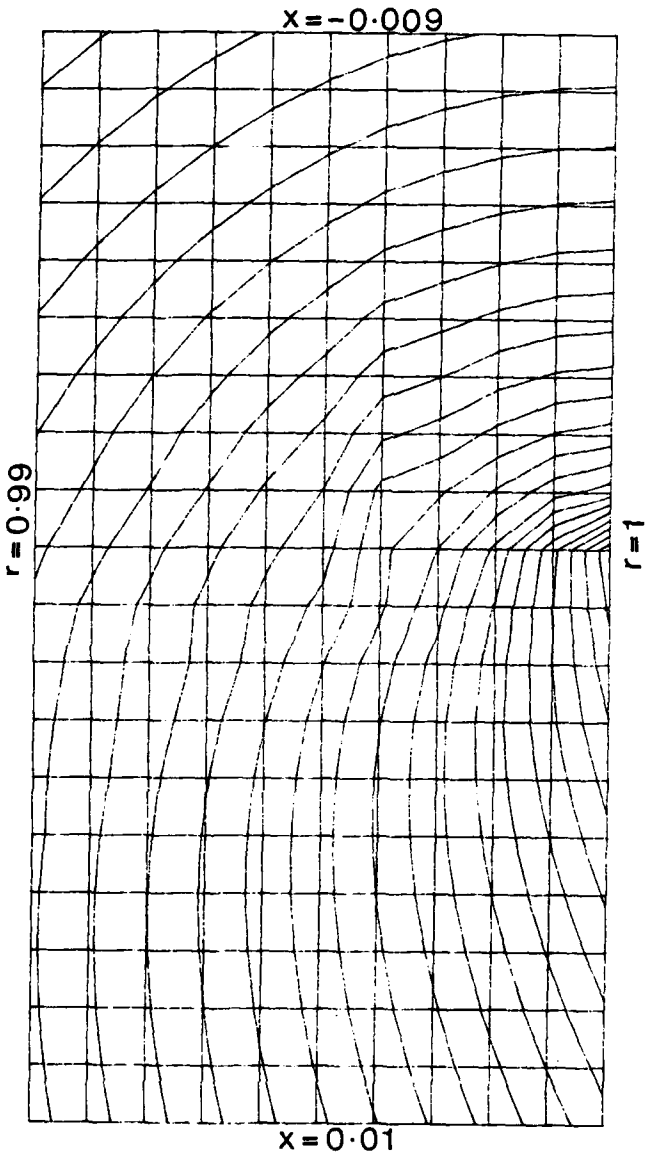

Fig 6 As Figs 4 and 5, detail very near lip, 0.33(0.08)2.01

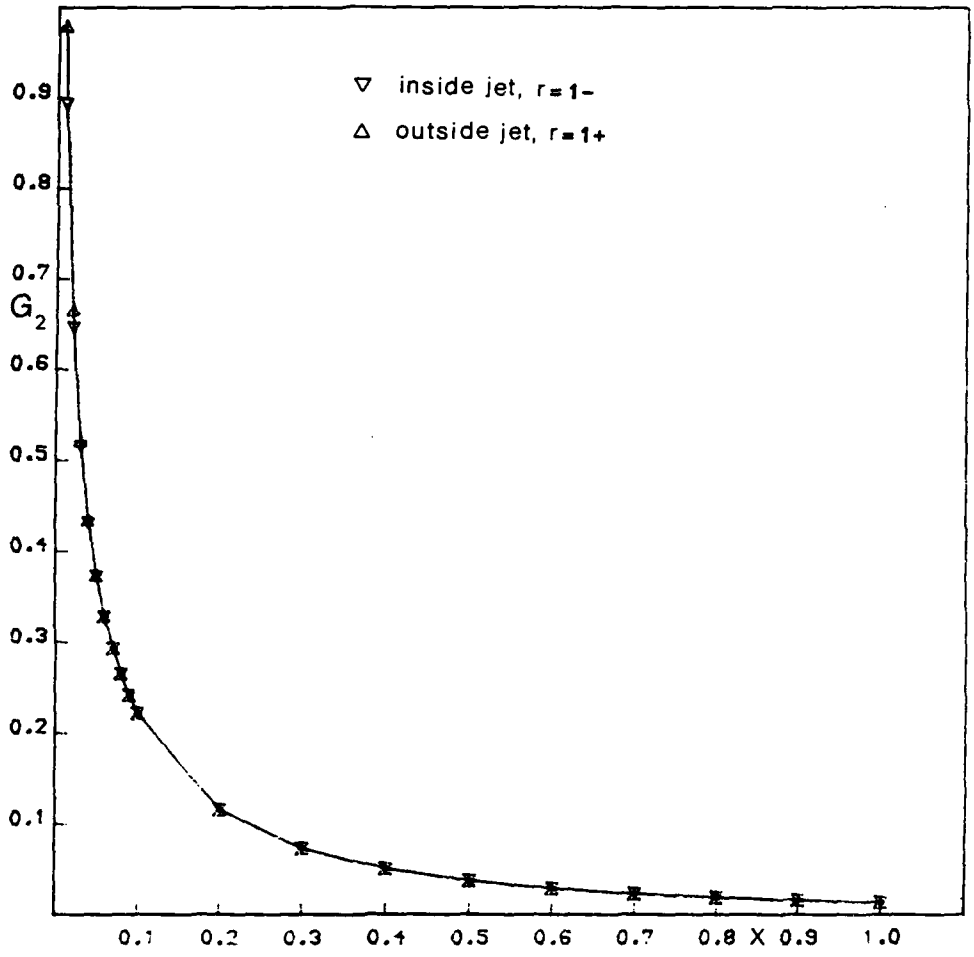

Fig 7 Comparison of normal derivatives from solutions inside and outside jet on the jet boundary

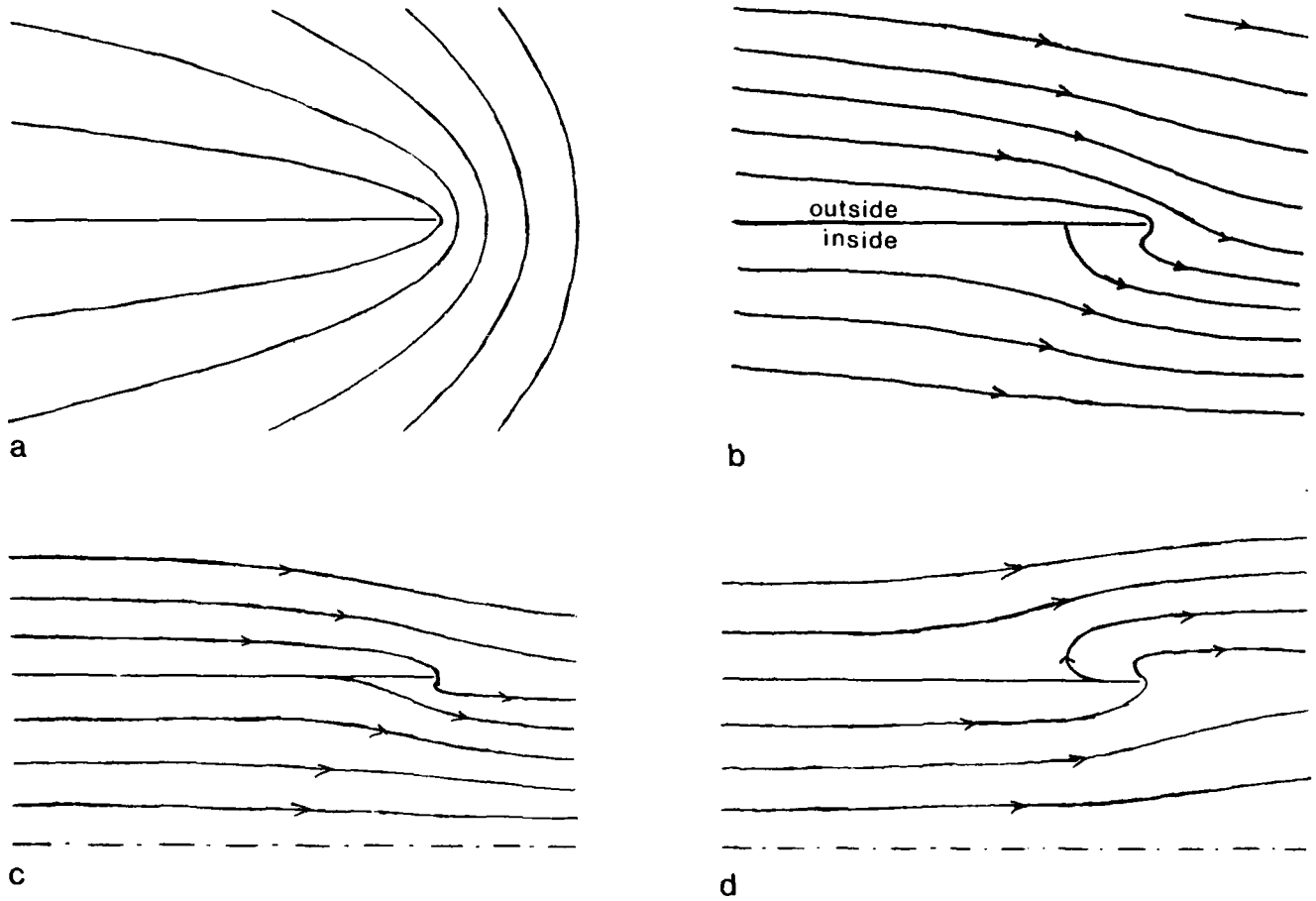

Fig 8 Streamline patterns: (a) semi-infinite plate, (b) local behaviour near lip for $\theta = \pm\pi/2$, (c) $\theta = \pm\pi/2$, with different total pressures (distorted scales), (d) as (c) for $\theta = 0, \pm\pi$

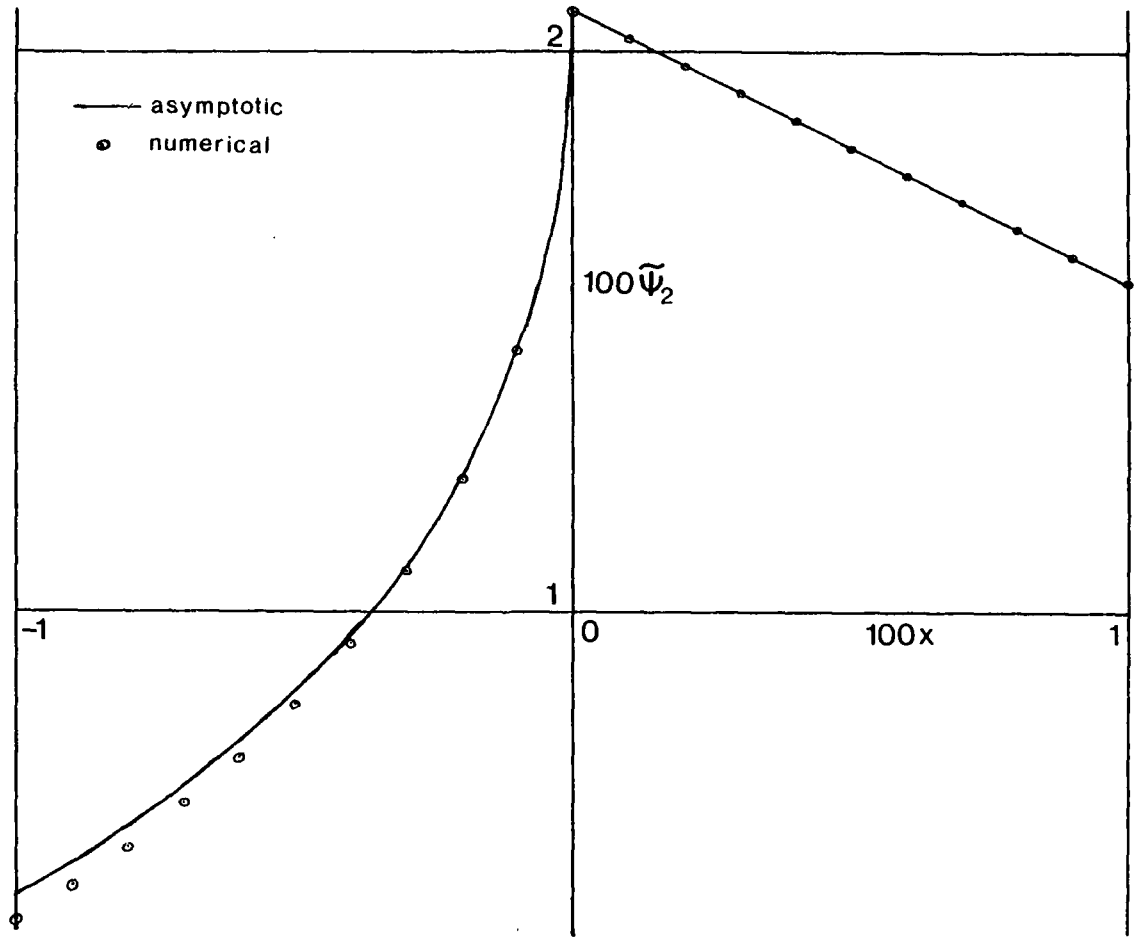

Fig 9 Comparison of numerical and asymptotic solutions on r = 1, very near lip

Fig 9

Fig 10

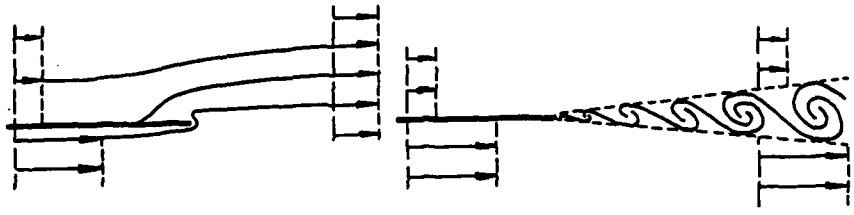

Fig 10 Conversion of a flow with an edge singularity (left) into a flow satisfying a Kutta condition (right). After Küchemann[5,6]

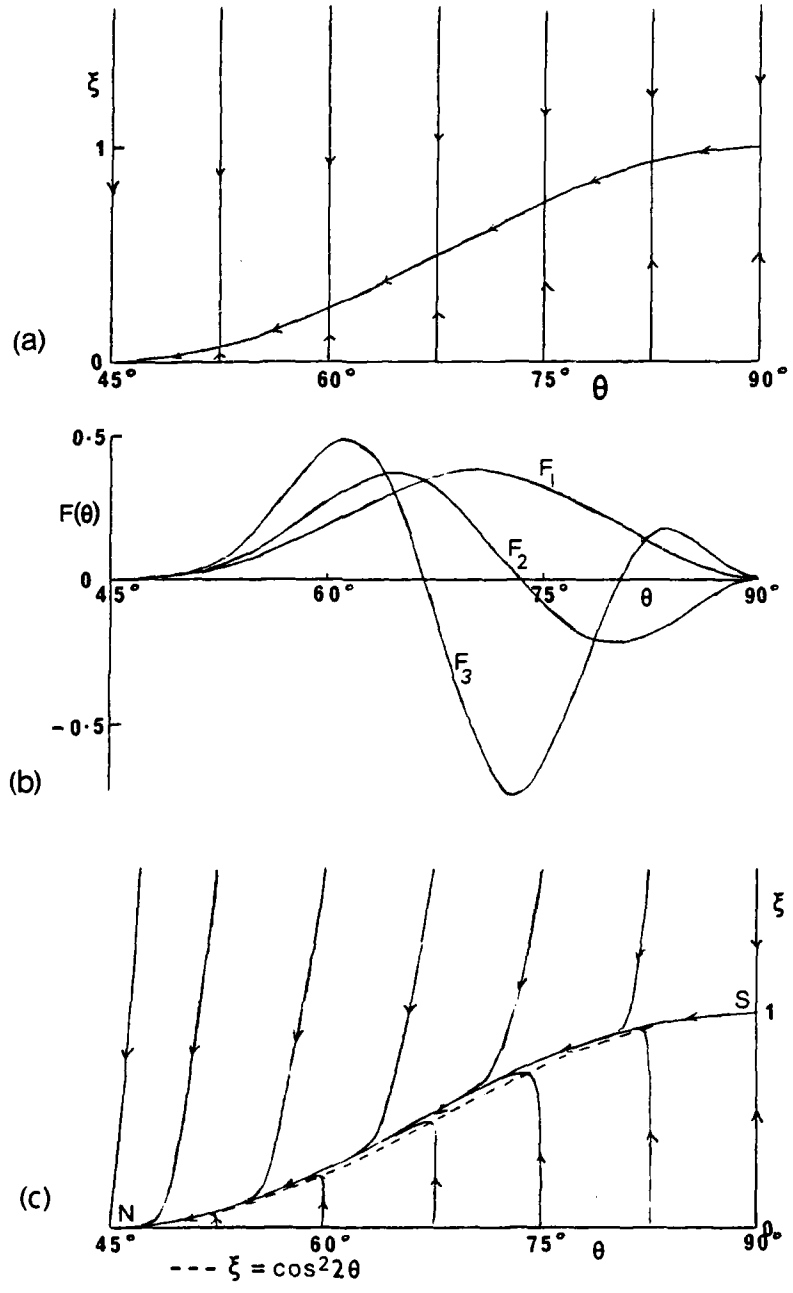

Fig 11 Surface streamlines just inside lip: (a) limiting case, $\delta = 0$; (b) auxiliary functions; (c) case with unrealistically large δ

Figs 12&13

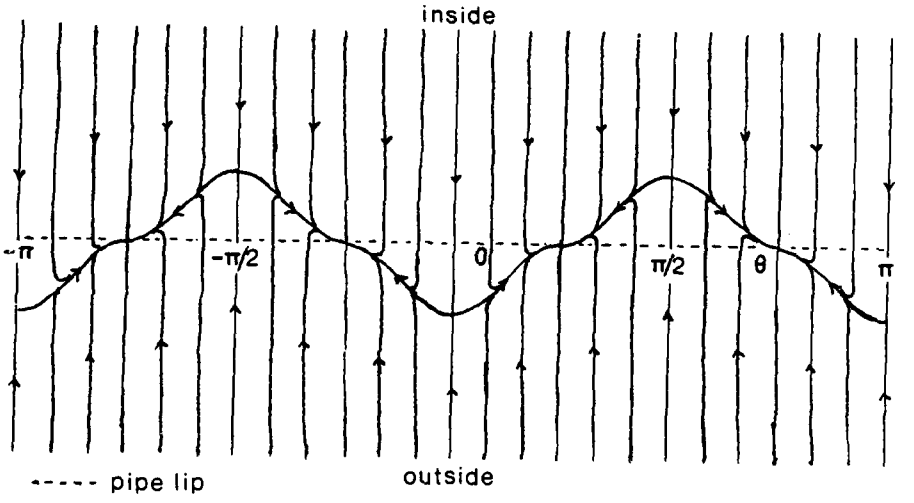

Fig 12 Surface streamlines near lip (vertical scale exaggerated)

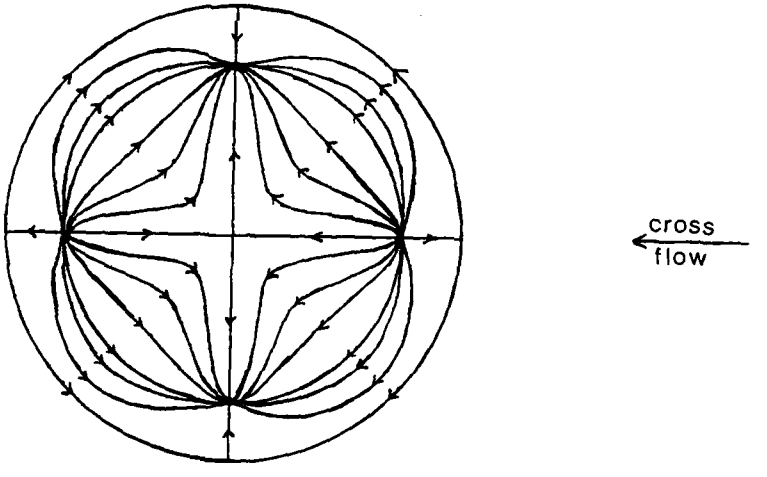

Fig 13 Secondary flow 'streamlines' inside pipe

REPORT DOCUMENTATION PAGE

Overall security classification of this page

UNLIMITED

As far as possible this page should contain only unclassified information. If it is necessary to enter classified information, the box above must be marked to indicate the classification, e.g. Restricted, Confidential or Secret.

1. DRIC Reference (to be added by DRIC)	2. Originator's Reference	3. Agency Reference	4. Report Security Classification/Marking
	RAE TM Aero 2137		UNLIMITED

5. DRIC Code for Originator	6. Originator (Corporate Author) Name and Location
7673000W	Royal Aerospace Establishment, Farnborough, Hants, UK
5a. Sponsoring Agency's Code	6a. Sponsoring Agency (Contract Authority) Name and Location

7. Title Numerical evaluation of a solution representing a jet in cross-flow

7a. (For Translations) Title in Foreign Language

7b. (For Conference Papers) Title, Place and Date of Conference

8. Author 1. Surname, Initials	9a. Author 2	9b. Authors 3, 4	10. Date	Pages	Refs.
Lytton, C.C.	Smith, J.H.B.		August 1988	49	8
11. Contract Number	12. Period	13. Project	14. Other Reference Nos.		

15. Distribution statement

(a) Controlled by – Head, Aero Department, RAE

(b) Special limitations (if any) –

If it is intended that a copy of this document shall be released overseas refer to RAE Leaflet No.3 to Supplement 6 of MOD Manual 4.

16. Descriptors (Keywords) (Descriptors marked * are selected from TEST)

Incompressible flow*. Inviscid flow*. Jets*. Jet in cross-flow.

17. Abstract

A recent study by Needham, Riley and Smith of a jet emerging from a circular pipe into a weak cross-flow under the assumptions of an inviscid and incompressible fluid led to expressions for the velocity potential in different regions near the orifice as definite integrals and infinite sums. In the present paper the expressions relating to flow inside the pipe and jet are evaluated with great care. It is confirmed that the solutions in the pipe and jet are continuous across the orifice plane. The behaviour of the solution near the orifice is displayed in graphical form, with emphasis on the consequences of the failure to satisfy a Kutta condition of smooth outflow at the lip.